Pathologe 2021 · 42:631–648
https://doi.org/10.1007/s00292-021-01012-w
Online publiziert: 13. Oktober 2021


# 2nd Swiss Pathology Days

## 87th Annual Congress of the Swiss Society of Pathology

November 4–6, 2021
Kursaal Interlaken

Dr. Dominik Loiero
Prof. Dr. Gieri Cathomas

Congress President
President SGPath-SSPath

## Orals

### O 1
### Development of novel prostate cancer patient-derived models and applications for translational research*

Raphaelle Servant*[1], Michele Garioni[1], Tatjana Vlajnic[2], Heike Pueschel[3], David C. Mueller[3], Tobias Zellweger[4], Arnoud J. Templeton[5], Andrea Garofoli[6], Sina Maletti[7], Zoi Diamantopoulou[8], Salvatore Piscuoglio[9], Mark A. Rubin[10], Nicola Aceto[8], Helge Seifert[3], Cyrill A. Rentsch[3], Lukas Bubendorf[2], Clementine Le Magnen[1]

[1]Department of Pathology, Institute of Medical Genetics and Pathology, and Department of Urology, University Hospital Basel, Basel, Switzerland; [2]Department of Pathology, Institute of Medical Genetics and Pathology, University Hospital Basel, Basel, Switzerland; [3]Department of Urology, University Hospital Basel, Basel, Switzerland; [4]Division of Urology, St. Clara Hospital, Basel, Switzerland; [5]Division of Medical Oncology, St. Claraspital, Basel, and Faculty of Medicine, University of Basel, Basel, Switzerland; [6]Pathology, Institute of Medical Genetics and Pathology, University Hospital Basel, and Visceral Surgery and Precision Medicine Research Laboratory, Department of Biomedicine, University of Basel, Basel, Switzerland; [7]Department for BioMedical Research, University of Bern, Bern, Switzerland; [8]Department of Biology, Institute of Molecular Health Sciences, Swiss Federal Institute of Technology (ETH) Zurich, Zurich, Switzerland; [9]Department of Pathology, Institute of Medical Genetics and Pathology, University Hospital Basel, and Visceral Surgery and Precision Medicine Research Laboratory, Department of Biomedicine, University of Basel, Basel, Switzerland; 1[9]Department for BioMedical Research, University of Bern, Bern, Switzerland and Bern Center for Precision Medicine, University of Bern and Inselspital, Bern, Switzerland

**Background:** Prostate cancer (PCa) translational research has been hampered by the scarcity of patient-derived models of hormone naïve (HN) disease. Here we present the successful establishment of a patient-derived organoid (PDO) line from a HN metastasis and subsequent development of PDO-Xenografts.
**Methods:** We attempted to derive organoids from 137 primary PCa or metastasis samples obtained from 131 PCa patients with diverse pathological and clinical features. Organoid growth was assessed using bright-field imaging and was correlated with histological features of the matched tumor samples. Tumorigenicity in vivo was assessed by subcutaneous injection in NOD scid gamma (NSG) mice. Matched tumor-organoid-xenograft samples were characterized using immunohistochemistry, immunofluorescence, and genomic sequencing. Cell viability after drug treatment was measured using CellTiter-Glo 3D.
**Results:** We identified improved experimental strategies favoring the generation of organoids derived from primary PCa specimens. Yet cancer-like organoids were progressively overgrown by benign-like organoids or quickly stopped growing in culture. Out of 21 PCa metastasis specimens, we established 7 short-term organoid cultures and one stable organoid model which was maintained in culture for more than 7 months. This novel organoid model was derived from a hormone-naive lung metastasis (P20-11) and displayed alterations in the PI3K/Akt and Wnt/β-catenin pathways and androgen sensitivity ex vivo. Patient-derived organoid xenografts (PDOX) were established upon subcutaneous injection of P20-11 organoids in NSG mice and recapitulated molecular features of the original patients' tumor and injected PDO. Organoids were grown from P20-11 PDOX and displayed androgen dependency ex vivo, as well as different degrees of response to androgen receptor signaling and AKT inhibitors.
**Conclusions:** We have successfully generated short-term PCa organoid cultures and established a novel PDO model of hormone-naïve advanced PCa. This model responds to androgen-targeted therapies and is tumorigenic in vivo,thereby representing a promising tool to study mechanisms of PCa progression and treatment response.
*Student paper

### O 2
### Establishing an immune diagnosis of metastatic melanoma with digital pathology

Bettina Sobottka[1], Marta Nowak* [1], Anja Frei[1], Martina Haberecker[1], Samuel Merki[1], Tu-Pro Tumor Profiler Consortium[2], Mitchell Levesque[3], Holger Moch[4], Viktor H. Kölzer[5]

[1]Department of Pathology and Molecular Pathology, University Hospital Zurich, University of Zurich, Zurich, Switzerland; [2]Tumor Profiler Consortium, Consortium, Switzerland [3]Department of Dermatology, University Hospital Zurich, University of Zurich, Zurich, Switzerland; [4]Department of Pathology and Molecular Pathology, University Hospital Zurich, University of Zurich, Zurich, Switzerland [5]Department of Pathology and Molecular Pathology, University Hospital and University of Zurich, Zurich, Switzerland

**Background:** CD8+ tumor-infiltrating T cells (CD8+ TILs) are regarded as one of the most relevant predictive biomarkers in immune-oncology. So-called inflamed tumors (clinically "hot") exhibit high CD8+ infiltration and show the most favorable response to immune checkpoint inhibitors. In contrary, tumors with absent or stroma-limited infiltrates, referred to as excluded or desert (clinically "cold"), show poor or no response. However, reproducible diagnostic methods quantifying CD8+ TILs prevalence within tumors are lacking. We therefore established an AI-based digital algorithm to quantify spatial distribution of CD8+ TILs and classify metastatic melanoma into clinically relevant immune phenotypes.
**Methods:** CD8+ TILs densities were measured in 114 metastatic melanomas of the Swiss Tumor Profiler cohort using a computational workflow

Die mit Sternchen (*) markierten Autoren sind die korrespondierenden Autoren.

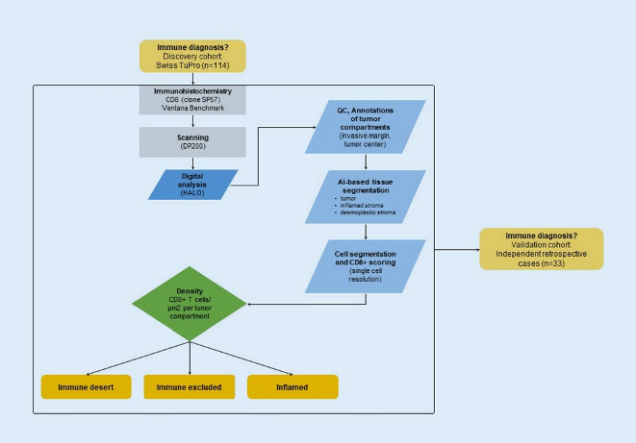


**Fig. 1 | O 2**

established using the image analysis platform HALO® (Indica Labs). Infiltrates were assessed based on spatial localization in three known tumor compartments defined according to international guidelines. Pre-analytical and analytical workflow robustness was confirmed in 33 samples of an independent retrospective validation cohort (**Fig. 1**).
**Results:** Digitally measured CD8+ TILs densities confirmed their differential spatial distribution among immune phenotypes in all assessed samples. The findings were highly reproducible in both cohorts. Based on defined cut-off values, densities of the validation cohort could be successfully assigned into the respective immune category. Introduction of the intratumoral cellular and stromal tumor center subcompartments proved to be most relevant for determining an immune diagnosis in metastatic disease, independent of metastatic site.
**Conclusion:** Herewith, we provide a robust diagnostic algorithm quantifying spatial distribution of CD8+ TILs. Our method allows reproducible classification of cases into the clinically relevant immune diagnostic categories "inflamed", "excluded" and "desert". The consideration of only tumor center subcompartments allows immune phenotyping in the clinically highly relevant setting of metastatic lesions, even if the invasive margin compartment is not captured in biopsy material.

## O 3
## Fully automated tumor infiltrating lymphocyte scoring pipeline in triple negative breast cancer demonstrates agreement with expert readers

Cédric Walker* [1], Hugo Horlings[2], Joyce Sanders[3], Sabine Linn[4], Sven Rottenberg[5], Andrew Janowczyk[6]

[1]University of Bern, Institute of Animal Pathology, Vetsuisse Faculty, Bern, Switzerland; [2]Netherlands Cancer Institute, Division of Molecular Pathology, Amsterdam, the Netherlands; [3]Netherlands Cancer Institute, Core Facility Molecular Pathology & Biobanking, Amsterdam, the Netherlands; [4]Netherlands Cancer Institute, Department of Medical Oncology, Amsterdam, the Netherlands; [5]University of Bern, Institute of Animal Pathology, Vetsuisse Faculty, Bern, Switzerland; Netherlands Cancer Institute, Division of Molecular Pathology, Amsterdam, the Netherlands; University of Bern, Bern Center for Precision Medicine, Bern, Switzerland; [6]Lausanne University Hospital, Precision Oncology Center, Vaud, Switzerland; Case Western Reserve University, Department of Biomedical Engineering, Cleveland OH, USA

**Background:** Tumor Infiltrating Lymphocyte (TIL) scoring has gained notable attention with the recent introduction of scoring guidelines by the international immuno-oncology working group [1]; additionally demonstrating prognostic and predictive significance in triple-negative breast cancer (TNBC). Unfortunately, studies have shown onerous manual TIL scoring suffers from intra/inter-observer variability [2]. Here a proof-of-concept for a reproducible, fully automatic, quantitative TIL scoring pipeline is presented.

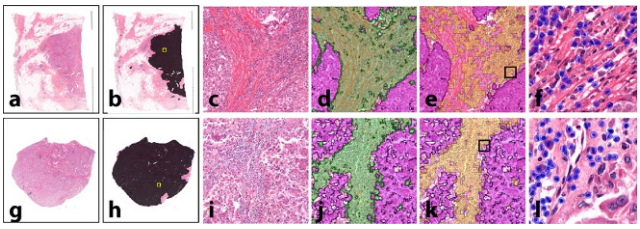


**Fig. 1 | O 3** ▲ Fig. 1 shows (**a** + **g**) original WSI, (**b** + **h**) the tumor bed estimation (*black*), as well as corresponding 400 × 400 ROIs at 10 × extracted from annotation (*yellow box*) in (**b** + **k**) showing (**c** + **i**) original H&E (**d** + **j**) with overlayed tumor (purple) and stroma (*green*) and (**e** + **k**) with overlayed tumor (*purple*) and TILs with 2 or more lymphocytes in a 128 × 128 sliding window with 64 stride (*yellow*). (**f** + **l**) show 500 × 500 ROIs at 40 × magnification with detedted lymphocytes (blue). Location of (**f** + **l**) corresponds to indicates region (*black box*) in (**e** + **k**)

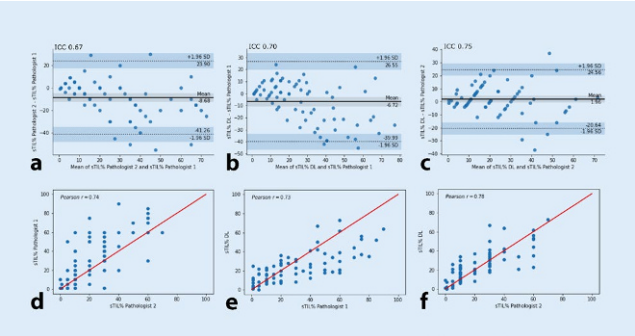


**Fig. 2 | O 3** ▲ Fig. 2 shows bland altman plot and scatter plot with identity line (*red*) for (**a and c**) pathologist 1 and pathologist 2, (**b and e**) pathologist 1 and our pipeline and (**c and f**) for pathogolist 2 and our pipeline

**Methods:** Our approach sees the employment of 4 deep learning (DL) models: (1) tumoral and (2) stromal regions are first delineated using models at 20 × with 64 × 64 patches. (3) To aid in mitigating false positives, a model was trained on normal glands and acted as an exclusionary mask. (4) Lymphocyte detection was trained using nuclei segmented by StarDist [3], and annotated as lymphocyte or non-lymphocyte using PatchSorter. Stromal TIL percentage (sTIL%) is defined as the percentage of stroma containing TILs (i. e., two or more lymphocytes are within a 128 × 128 window using 64 stride) divided by the tumor bed area (estimated by applying dilation on the detected tumor mask). A test-set of 58 TNBC slides from the MATADOR [4] cohort was scored by two pathologists according to established guidelines [1]. For statistical non-inferiority, significance margin was set based on published inter-observer studies (δ = 0.83) [2].
**Results:** Visual assessment showed good quality in nuclei, lymphocytes, tumor, and stroma classification (**Fig. 1**). Intra-Class Correlation (ICC) between the two pathologists is 0.67 demonstrating high intra-observer variability in TIL scoring (**Fig. 2**). ICC between the DL pipeline and pathologists are 0.70/0.75. Differences between ICC are within defined non-inferiority margins, suggesting comparability of our method to expert manual assessment.
**Conclusion:** Our preliminary results suggest our method offers a robust, accurate, and reproducible fully automatic pipeline for TIL scoring. Given the single cell resolution, this pipeline also has the potential to help in further characterizing patterns of immune infiltration in breast cancer.

## References

1. Salgado R, Denkert C, Demaria S et al (2015) The evaluation of tumor-infiltrating lymphocytes (TILs) in breast cancer: recommendations by an International

TILs Working Group 2014. Ann Oncol 26(2):259–271. https://doi.org/10.1093/annonc/mdu450
2. O'Loughlin M, Andreu X, Bianchi S, et al (2018) Reproducibility and predictive value of scoring stromal tumour infiltrating lymphocytes in triple-negative breast cancer. a multi-institutional study. Breast Cancer Res. Treat 171(1):1–9. https://doi.org/10.1007/s10549-018-4825-8
3. Weigert M, Schmidt U, Haase R, Sugawara K, Myers G (2020) Star-convex Polyhedra for 3D Object Detection and Segmentation in Microscopy. In: 2020 IEEE Winter Conference on Applications of Computer Vision (WACV). IEEE:3655–3662. https://doi.org/10.1109/WACV45572.2020.9093435
4. van Rossum AGJ, Kok M, McCool D et al (2017) Independent replication of polymorphisms predicting toxicity in breast cancer patients randomized between dose-dense and docetaxel-containing adjuvant chemotherapy. Oncotarget 8(69):113531–113542. https://doi.org/10.18632/oncotarget.22697

## O 4
## The needle in a haystack: identification of pathogens in human FFPE tissue samples by shotgun WGS and metagenomics analysis

Ronny Nienhold*, Nadine Mensah, Angela Frank, Anne Graber, Jacqueline Koike, Nathalie Schwab, Claudia Hernach, Gieri Cathomas, Kirsten Mertz

Kantonsspital Baselland, Basel, Switzerland

**Background:** Pathologists frequently encounter samples from patients infected with unknown pathogens. The identification of microorganisms in formalin fixed paraffin embedded (FFPE) tissue samples is based on: (1) Microscopic assessment of tissue morphology; (2) Species-specific PCRs to identify pathogenic microorganisms. However, the available PCR assays cover only a limited set of frequent pathogens and rare infectious agents are hard to detect.
**Methods:** To identify a broad spectrum of pathogens from DNA of FFPE tissue samples, we established a whole genome sequencing (WGS) approach that combines shotgun sequencing and metagenomics analysis. This analysis utilizes non-human reads, from which pathogens are identified by taxonomic profiling.
**Results:** To validate the assay, we analyzed more than 200 samples, including dilution series of mock communities, autopsy and biopsy FFPE tissue samples with previously confirmed bacterial infections.
Compared to data acquired from microbiome analysis of the gut, metagenomics analysis of infections display low complexity and display less than 5 bacterial genera in 95 % of biopsy samples and 86 % of autopsy samples. In the majority of biopsies (61 %) and a large fraction of autopsy samples (38 %) only one single bacterial species was detected, in line with morphological appearance of tissues.
In the majority of autopsy and biopsy samples (59 % and 55 % respectively), metagenomics WGS identified pathogenic species, which were confirmed by species-specific PCRs. The lower level of detection was 100 bacterial genomes. This novel method also uncovered previously unidentified pathogens in samples, which had been tested negative for multiple common microorganisms.
**Conclusions:** The metagenomics WGS assay is a sensitive, quantitative and unbiased approach allowing identification of unknown pathogens in FFPE tissue samples.

## O 5
## Microvascular dysfunction, plasmablast accumulation, proinflammatory macrophage activation and aberrant t-cell response in pulmonary lymph nodes of COVID-19

Jasmin Haslbauer* [1], Matthias Matter[1], Carl Zinner[2], Anna Stalder[1], Jan Schneeberger[1], Thomas Menter[1], Kirsten Mertz[3], Philip Went[4], Alexandar Tzankov[1]

[1]Pathology, Institute of Medical Genetics and Pathology, University Hospital Basel, University of Basel, Switzerland; [2]Institute of Biomedicine, University of Basel, Basel, Switzerland [3]Department of Pathology, Kantonsspital Baselland, Basel, Switzerland [4]Department of Pathology, Kantonsspital Graubünden, Graubünden, Switzerland

**Background:** Initial immunophenotypical studies on peripheral blood and bronchoalveolar lavage samples have provided a glimpse into the immunopathology of COVID-19, yet analyses of pulmonary draining lymph nodes are currently scarce.
**Methods:** 21 lethal COVID-19 cases and 31 controls were enrolled. Pulmonary draining lymph nodes (mediastinal, tracheal, peribronchial) of COVID-19 cases were collected at autopsy. Control lymph nodes were selected from a range of histomorphological sequelae [unremarkable histology, infectious mononucleosis, follicular hyperplasia, non-SARS related hemophagocytic lymphohistiocytosis (HLH), extrafollicular plasmablast

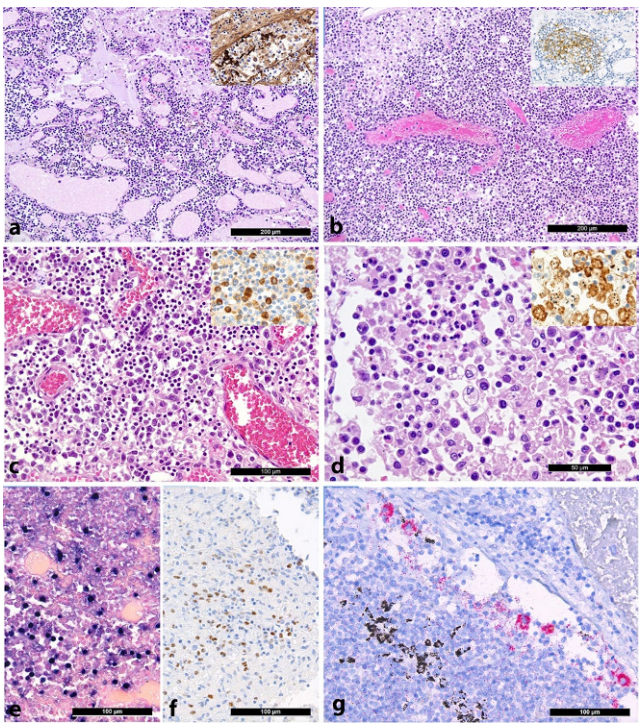


**Fig. 1 | O 5 ▲ a** Overview of a lymph node draining a COVID-19 lung with edema and capillary stasis (H&E; 50×); inlet: fibrin microthrombus in a dilated subcapsular sinus (immunoperoxidase; 50×). **b** Severe capillary stasis and expansion of the paracortex without discernable germinal centers (H&E; 100×); inlet: disrupted CD21 + germinal center structure (immunoperoxidase; 100×). **c** Proliferation of extrafollicular plasmablasts (H&E; 200×); inlet: expression oflgM by the plasmablasts (immunoperoxidase; 360×). **d** Hemophagocytosis in the sinus of a lymph node (H&E; 360x); inlet: positivity for CD11c in histiocytes undergoing HLH (immunoperoxidase; 400×). **e** Increased amount ofEBV infected B-cells in a lymph node of a COVID-19 patient (EBER in situ hybridization; 280x). **f** Increased amount ofHSV infected B-cells (immunoperoxidase; 280x). **g** SARSCoV -2 positivity in sinus histiocytes as detected by IHC for the SARS-Co V -2 Nantigen (immunoperoxidase with 3-amino-9-ethylcarbazole used as a chromogen;280×)

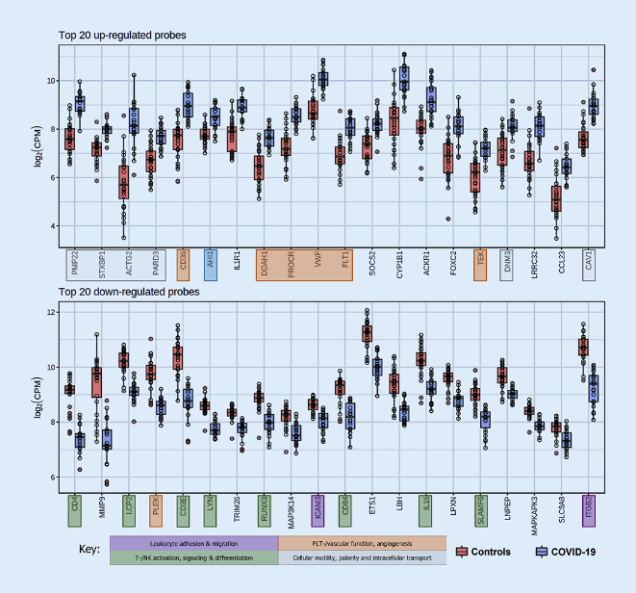


**Fig. 2 | O 5** ▲ Characteristic gene expression profiling of COVID-19 immunology. **a**) Principal component analysis showing distinct clustering of COVID-19 and controls. **b**) Top 20 up-regulated genes in COVID-19 versus controls: genes related to cellular structure, motility and intracellular transport, proangiogenic and prothrombotic genes were predominantly upregulates in COVID-19. Genes involved in T-/NK- and B-cell differntiation and signaling and leukocyte trafficking were predominantly down-regulated in COVID-19

activation, non-SARS related diffuse alveolar damage (DAD), pneumonia]. Samples were mounted on a tissue microarray and underwent immunohistochemical stainings for immune cell markers and in-situ hybridization for Epstein Barr Virus (EBV) and SARS-CoV-2. Gene expression profiling was performed using the HTG EdgeSeq Immune Response Panel.
**Results:** Characteristic patterns of a dysregulated immune response were detected: 1. Microvascular dysfunction, evidenced by dilatation of sinuses, an upregulation of hemostatic (CD36, PROCR, VWF) and proangiogenic (FLT1, TEK) genes and an increase of fibrin microthrombi (**Fig. 1**a,b and 2). 2. Accumulation of extrafollicular plasmablasts in lieu with a relative paucity or depletion of germinal centers (**Fig. 1**b,c). 3. Macrophage activation by a proinflammatory, CD163+ phenotype and increased incidence of hemophagocytic activity (**Fig. 1**d). 4. Evidence of T-cell dysregulation demonstrated by a reactivation of herpes viruses in 6/21 COVID-19 lymph nodes (EBV, HSV) (**Fig. 1**e), decrease of Tregs and TH1 cells and downregulation of key genes responsible for T-cell crosstalk, maturation and migration (**Fig. 2**). Unsupervised cluster analysis of differentially expressed genes revealed a unique pattern of 46 deregulated genes in the draining lymph nodes of COVID-19, which support the 4 patterns of response explicated above (**Fig. 3**).
**Conclusion:** Our findings imply widespread dysregulation of both innate and adaptive pathways with concordant microvascular dysfunction in severe COVID-19.

## O 6
## HRD scoring with SNP assays

Yann Christinat*, Liza Ho, Sophie Clément Leboube, Thomas McKee

Hôpitaux universitaires de Genève, Genève, Switzerland

**Background:** Homologous recombination deficiency (HRD) is a well-known characteristic of BRCA-mutated tumors, an alteration present in ~30 % of ovarian cancers and also in certain breast, prostate and pancreatic cancers. The PAOLA-1 trial demonstrated that responders to PARP inhibitors do not only include BRCA-mutated tumors but also tumors that are BRCA-wildtype but display an HRD phenotype and many different scores and technologies have been proposed and commercialized to assess HRD. Nonetheless, many of these solutions are complicated to implement and/or expensive.
**Methods:** We propose a novel HRD scoring algorithm based copy number alterations obtained from a clinicalgrade SNP assay designed to analyse FFPE samples (ThermoFisher Oncoscan Assay). The method has been evaluated on 400 high-grade ovarian carcinoma and 100 triple-negative breast cancer samples from the TCGA cohort. A validation was performed on an internal cohort of 50 ovarian cancers.
**Results:** The algorithm performed better than two well-known commercial methods, the compound score from Telli et al. (LST+LOH+TAI) and the percentage of LOH bases across the genome, and classified correctly the BRCA-mutated cancers into the HRD category.
**Conclusion:** The high concordance with the LST+LOH+TAI score led to its inclusion into the clinical routine at the Geneva University Hospitals. The method is also being evaluated as a biomarker to predict response to Olaparib as part of the phase 3 of the ENGOT HRD European Initiative (EHEI).

## O 7
## Reducing the annotation workload: using self-supervised methods to learn from publicly available colorectal cancer datasets*

Christian Abbet* [1], Linda Studer* [2], Andreas Fischer[2], Behzad Bozorgtabar[1], Jean-Philippe Thiran[1], Felix Müller[3], Heather Dawson[4], Inti Zlobec[5]

[1]Signal Processing Lab 5 (LTS5), EPFL, Lausanne, Lausanne, Switzerland [2]iCoSys, Hochschule für Technik und Architektur Freiburg, Freiburg, Switzerland [3]University of Bern, Institute of Pathology, Bern, Switzerland [4]Institute of Pathology, University of Bern, Bern, Switzerland [5]Universität Bern, Bern, Switzerland

**Background:** Supervised learning is constrained by the availability of labeled data, which are especially expensive to acquire, as they are very time-consuming and need expert knowledge. Making use of open-source datasets and applying domain adaptation can be a way to overcome this issue. Combining the former with self-supervised learning, where "the data creates its own supervision", allows us to learn rich features from unlabeled data. We apply this method to tissue type detection, which is helpful for many downstream tasks such as the prediction of prognostic factors.
**Methods:** We use our proposed Self-Rule to Adapt (SRA) framework [1] to perform domain adaptation between an opensource colorectal cancer dataset [2] and our in-house H&E-stained adenocarcinoma cohort. Our architecture uses a two-step approach to build tissue representations. Firstly, the model learns domain agnostic features in a selfsupervised fashion. Secondly, the model takes advantage of the available open-source dataset to predict tissue classes, thus reducing the annotation workload for pathologists.
**Results:** To assess the quality of our model, we perform classification of selected tissue regions from our in-house cohort, which are annotated by an expert pathologist. The areas include challenging examples such as different cancer stages, desmoplastic reaction, and torn tissues. We compare our results with the standard supervised transferlearning baseline over various metrics. The proposed method achieves 68.2 %, 54.8 %, 58.7 % in terms of accuracy, weighted intersection over union, and pixel-wise Cohen's kappa score over nine classes against 51.4 %, 40.8 %, 41.7 % for the baseline.
**Conclusion:** We show that our proposed architecture can learn and classify complex tissue representations in an unsupervised manner, thus relieving the pathologists from tedious annotation work. As a result, it makes our algorithm a good candidate for future research where we rely on large sets of unlabeled scans, such as in CMS classification or tumor-stroma ratio quantification.
*Student paper

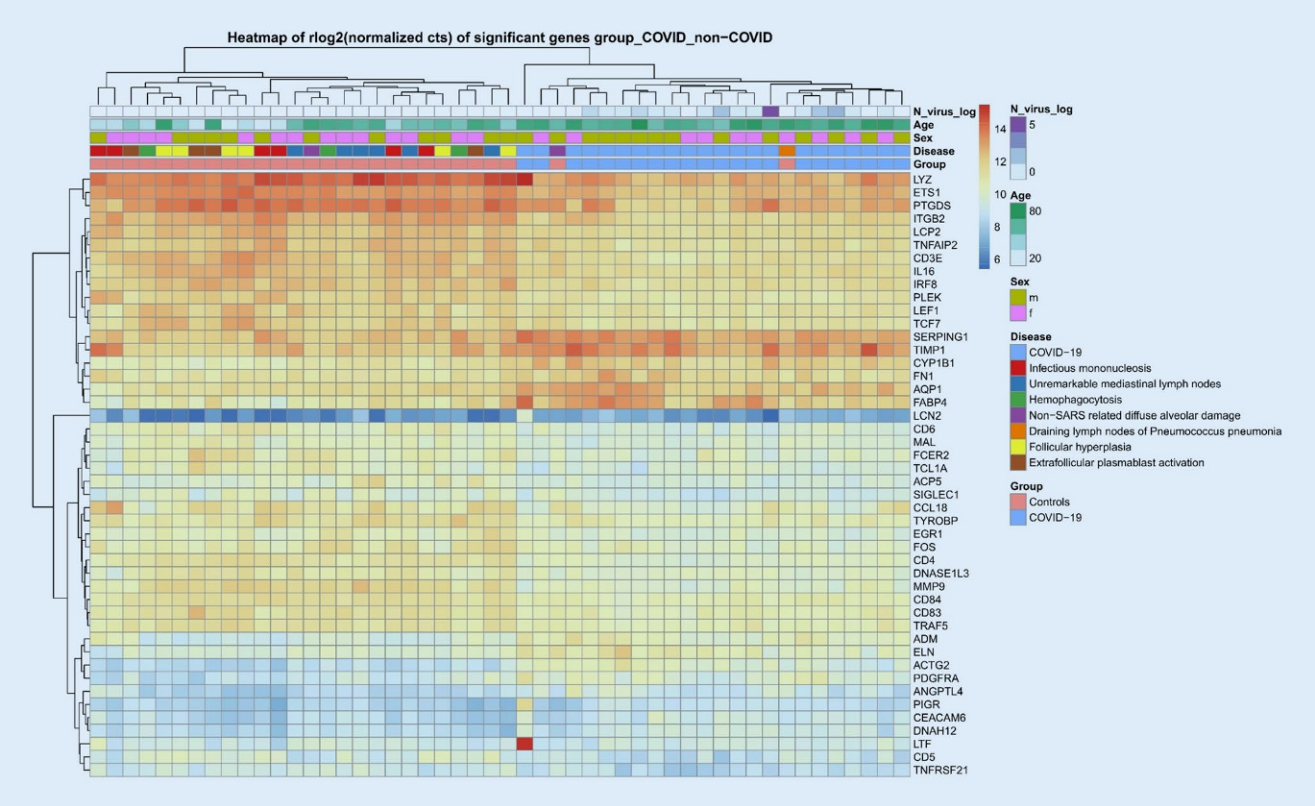


**Fig. 3 | O 5** ▲ Unsupervised cluster analysis of differentially expressed genes in the draining lymph nodes of COVID-19 and control cases. A downregulation of genes related to T-cell function and differentiation (LCP2, CD3E, LEF1, CD6, MAL, TCL1A, TYROBP, CD84, CD%), particulary related to CD4 cells (IL16, CD4), macrophage function (LYS, SIGLEC 1) and genes encoding for immunoglobulin receptors (FCER2, PIGR) was observed. Genes related to complement and fluid homeostasis and vascular functions (SERPING1, AQP1, ADM, ANGPTL4) were upregulated

## References


1. https://openreview.net/forum?id=VO7asaS5GUk
2. https://zenodo.org/record/1214456


## O 8
## Accelerating the annotation process of large whole slide image datasets


Maxime Lafarge* [1], Korsuk Sirinukunwattana[2], Enric Domingo[3], Jennifer Hay[4], Andrea Harkin[5], Andrew Blake[3], James Robineau[3], Owen Sansom[6], David Church[7], Ian Tomlinson[8], Joanne Edwards[9], Jens Rittscher[2], Tim Maughan[10], Viktor H. Kölzer[1]

[1]Department of Pathology and Molecular Pathology, University Hospital and University of Zurich, Zurich, Switzerland; [2]Institute of Biomedical Engineering (IBME), Department of Engineering Science, University of Oxford, Oxford, UK; [3]Department of Oncology, University of Oxford, Oxford, UK; [4]Glasgow Tissue Research Facility, University of Glasgow, Queen Elizabeth University Hospital, Glasgow, UK; [5]CRUK Clinical Trials Unit, The Beatson West of Scotland Cancer Centre, Gartnavel Hospital, Glasgow, UK; [6]Wolfson Wohl Cancer Research Centre, Institute of Cancer Sciences, University of Glasgow, United Kingdom.; [7]Wellcome Centre for Human Genetics, University of Oxford, Roosevelt Drive, Oxford, UK; [8]Edinburgh Cancer Research Centre, IGMM, University of Edinburgh, Edinburgh, UK; [9]Wolfson Wohl Cancer Research Centre, Institute of Cancer Sciences, University of Glasgow, UK; 1[0]MRC Oxford Institute for Radiation Oncology, University of Oxford, Oxford, UK



**Background:** The localization of the tumor microenvironment in histopathology images is a key step to facilitate the downstream analysis of colorectal cancer (CRC) cases. However, manually annotating large datasets (n > 3000) is a tedious task that requires time and expertise. Modern approaches to automate this task typically rely on machine learning segmentation solutions. Yet, applying a model previously trained on a given dataset will not necessarily generalize well to independent target cohorts. Here, we investigate an active learning procedure that automatically provides predictions of tumor regions for a subset of selected target images that annotators can easily manually correct. We iteratively use these generated annotations to improve and estimate the generalization performances of our segmentation models.


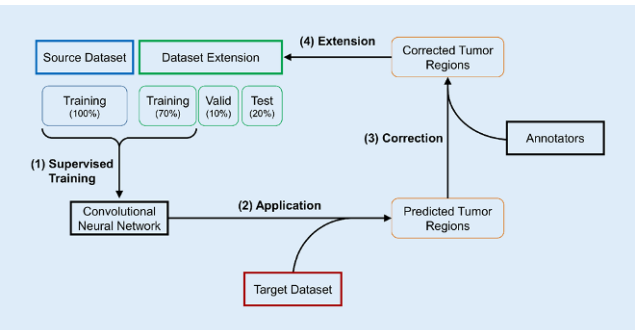


**Fig. 1 | O 8** ▲ Flowchart of the investigated active learning process. An ensemble of convolutional networks is trained using all available annotated images (1). Predicitions are generated for all non-annotated images (2), and are then selected based on an unvertainty heuristic (query-by committee) to be manually corrected by annotators (3). These manual corrections are then included as training data for the next generations of models (4)

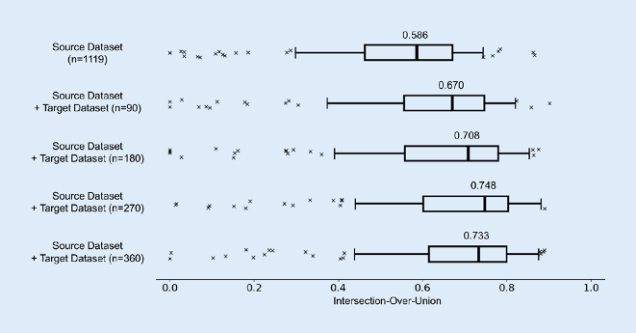


**Fig. 2 | O 8** ▲ Box plots of the performances (Intersection-Over-Union: area of the intersection divided by the area of the union os the predicted and ground-truth tumor regions) of our segmentation models on a fixed hold-out test set of the target dataset ($n = 90$). Performances are shown for varying qunatities of annotated target images used for training

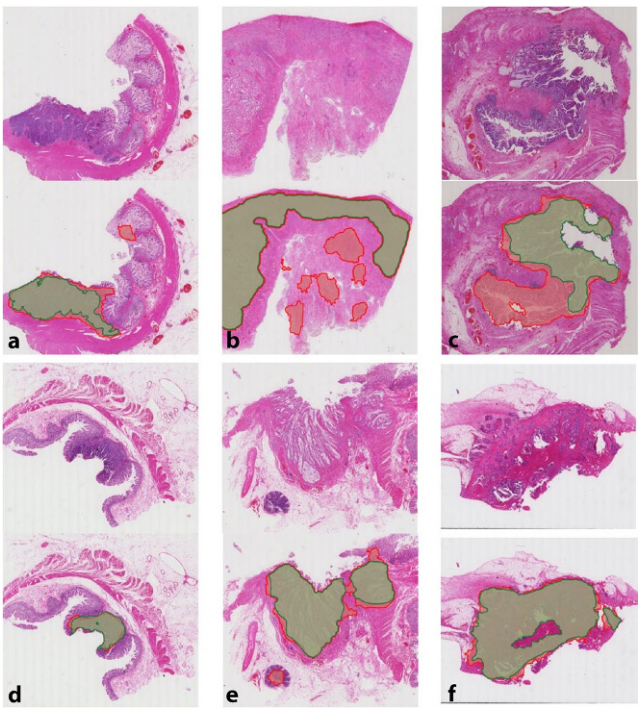


**Fig. 3 | O 8** ▲ Examples of the prediction/correction procedure on target images selected for their high predictive uncertainty. Tissue regions are shown with overlays of predicted tumor regions (*red*) and overlays of manual corrections (green). (**a, b, c**) Localized tumor regions with low IoU. (**d, e, f**) Localized tumor regions with high IoU that required minor corrections

**Patients and methods:** Our material consists of digitized slides of H&E-stained CRC cases: (a) source dataset of 1119 WSIs with annotated tumor regions (FOCUS, SPINAL, PT1, ARISTOTLE cohorts); (b) target dataset of 3218 WSIs (SCOT cohort). Both datasets include resection and biopsy samples. Our method consists of a procedure that iterates over the steps illustrated in the flowchart of (◘ **Fig. 1**): we alternatively trained generations of convolutional neural networks (U-Net) using available annotations, and identify non-annotated images based on an uncertainty heuristic that annotators are requested to correct.
**Results:** In a data regime analysis, we show that after three rounds of active learning, the newly annotated images ($n = 500$) enabled the estimation and improvement of performances of our segmentation models on the target dataset. Detailed performance statistics are provided in (◘ **Fig. 2**).
**Conclusions:** We confirm that active learning has a potential for supporting the rapid generation of new manual annotations. We report that it was faster to make corrections of predicted contours rather than generating annotations from scratch (◘ **Fig. 3**). This procedure enabled us to validate the applicability of our trained segmentation models for a large independent cohort.

## Posters

### P 1
### Renal post-mortem findings in myeloproliferative and myelodysplastic/myeloproliferative neoplasms

Fermin Person* [1], Sara Meyer[2], Helmut Hopfer[1], Thomas Menter[1]

[1]Pathology, Institute of Medical Genetics and Pathology, University Hospital Basel, University of Basel, Switzerland; [2]Department of Hematology, University Hospital Basel, Switzerland

**Background:** Myeloproliferative neoplasms (MPN) are a heterogeneous group of haematological disorders presenting with an increased proliferation in one or several haematological cell lines. Renal manifestations of MPN have not been fully characterized so far.
**Methods:** To morphologically assess the potential renal involvement in MPN patients, we analyzed histomorphological findings of a post-mortem cohort ($n = 57$) with a disease history of Philadelphia-negative MPN including polycythaemia vera, primary myelofibrosis, essential thrombocythemia, or chronic myelomonocytic leukaemia (CMML).
**Results:** Seven (12.2 %) patients presented with a pattern of diffuse glomerulosclerosis not attributable to diabetic or hypertensive nephropathy. Weak C4d staining suggestive for chronic thrombotic microangiopathy (TMA) was observed in 4/7 cases. Glomerulonephritis was excluded by light microscopy and immunohistochemistry. Patients with a pattern

| Findings | |
|---|---|
| Male/Female | 32/25 |
| Age | Mean: 74, Median: 77, Range: 33 – 96 years |
| Duration of disease | Mean: 7 years, Median: 3 years, Range: <1 - 50 years |
| Type of disease | CMML: 18<br>ET: 1<br>PV: 16<br>PMF: 16<br>MPN other: 6 |
| Haematopoetic cell transplantation | 11/57 |
| Cause of death | Cardiac disease: 11/57<br>HCT-related: 2/57<br>Infectious diseases: 27/57<br>Hemorrhagic shock: 4/57<br>Lung embolism: 9/57<br>Tumor progression: 4/57 |
| Kidney function* | G1: 17/55<br>G2: 27/55<br>G3a: 6/55<br>G3b: 3/55<br>G4: 2/55 |
| Idiopathic diffuse glomerulosclerosis | 7/57 |
| Diabetic Glomerulosclerosis | 2/57 |
| Diabetes | 2/57 |
| Arteriolosclerosis | 18/57 |
| Shock signs | 8/57 |
| Florid pyelonephritis | 2/57 |
| Extramedullary haematopoesis in the kidney | 5/57 |
| Infiltration of the kidney by blastoid cells | 3/57 |
| Other non-specific findings** | 29/57 |
| No renal involvement | 9/57 |

*: laboratory parameters were available of 55/57 patients

**: this includes simple cysts, small vascular scars, mild nephrocalcinosis and papillary adenoma

**Fig. 1 | P 1** ▲ General clnical characteristics and autopsy findings of our cohort

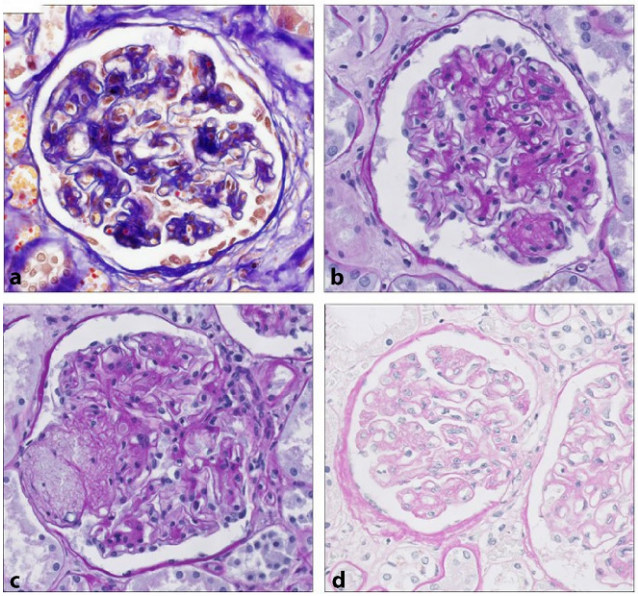

**Fig. 2 | P 1** ▲ Features of diffuse mesangial sclerosis. a and b: mesangial matrix expansion can be seen in the trichrome (**a**) and the PAS stain (**b**) (400×); **c**: another case of diffuse mesangial sclerosis showing mesangiolysis (arrow) hinting at chronic endothelial damage (11) (PAS, 400×); **d**: prominent wrinkling of glomerular capillary basement membranes in addition to mild mesangial matrix expansion also pointing at chronic TMA (PAS, 400×)

of diffuse glomerulosclerosis did not differ from the rest of the cohort regarding MPN subtype, disease duration, age or sex. No significant proteinuria had been observed before death. Further findings attributed to MPNs were extramedullary haematopoiesis ($n=5$; 8.8 %) and tumour involvement in advanced disease ($n=4$; 7.0 %). Other common findings included arteriolosclerosis ($n=18$; 31.6 %) and signs of shock ($n=8$; 14.0 %).
**Conclusions:** To our knowledge, this study is so far the largest investigating renal findings in MPN patients. There may be a causal relationship between idiopathic diffuse glomerular sclerosis and MPN, although its clinical significance and pathophysiology remain uncertain with TMA probably being relevant in a subgroup of cases. Our findings demonstrate the spectrum of renal findings in MPN from early to terminal disease of which haematologists should be aware of in daily clinical practice.

## P 2
## Clinicopathological features of cutaneous reactions after mRNA-based COVID-19 vaccines

Matthieu Tihy* [1], Sébastien Menzinger* [2], Raphaël André[3], Emmanuel Laffitte[1], Laurence Toutous-Trellu[1], Gürkan Kaya[2]

[1]Clinical Pathology, University Hospitals of Geneva, Geneva, Switzerland [2]Clinical Pathology, University Hospitals of Geneva; Dermatology Service, University Hospitals of Geneva, Geneva, Switzerland [3]Dermatology Service, University Hospitals of Geneva, Geneva, Switzerland

**Background:** In Switzerland, two COVID-19 vaccines are currently administered to the population: Pfizer and Moderna, with cutaneous adverse reactions reported for both. Moderna's trial reported delayed injection-site reactions, characterized by erythema, induration, and tenderness, called COVID arm. The most common reactions notified in an international registry were delayed large local reactions, followed by local injection site reactions, urticaria, morbilliform rash and erythromelalgia. Other reactions were swelling at the site of cosmetic fillers, pernio/chilblains, varicella-zoster, herpes-simplex flares, pityriasis rosea-like eruption and vasculitis. Our work attempts to make a clinicopathological description of cutaneous reactions to COVID-19 vaccines.

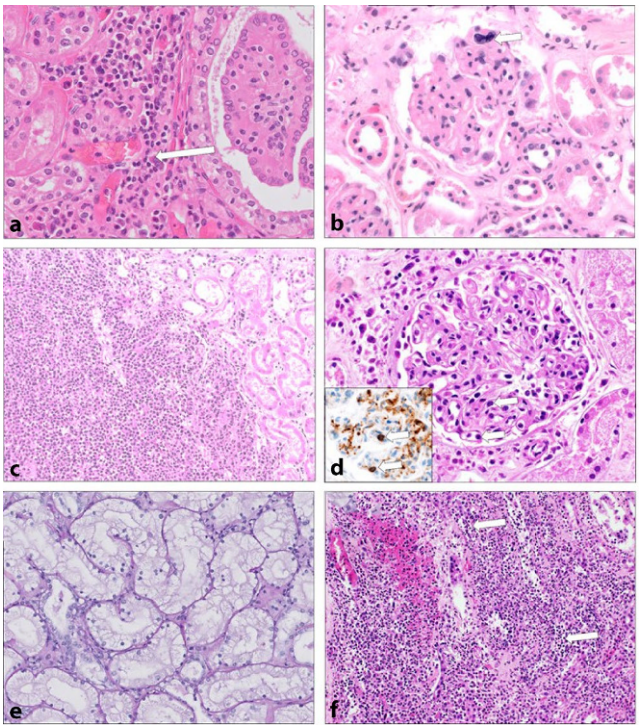

**Fig. 3 | P 1** ▲ Other morphologic findings in our cohort. **a**: focus of extramedullary haematopoiesis showing myeloid and erythroid cells as well as a megakaryocyte (arrow) (H&E, 400×). **b**: extramedullary haematopoiesis showing a megakaryocyte (arrow) in a capillary loop of the glomerulus (H&E, 400×); **c**: kidney infiltrates of blasts in a patient with transformation of PMF into AML (H&E, 200×); **d**: glomerulus showing intracapillary blasrs and myeloid precursors (arrow) of a case with transformation into AML (H&E, 400×), the insert confirms the blasts in a CD34 immunohistochemical stain (arrow, 400×); **e**: severe acute tubular damage of the osmotic nephrosis type showing fine-vaculoated cytoplasm of the tubuli (H&E, 200×); **f**: acute pyelonephritis showing a dense infiltrate of neutrophils destroying the basement membrane of tubuli (*arrow*) (H&E, 200×)

**Methods:** We performed a retrospective study to characterize clinical and histopathological aspects of skin reactions to both vaccines at University Hospital of Geneva. A skin biopsy was required for inclusion.
**Results:** Among 11 subjects, 8 received Pfizer and 3 Moderna vaccine. The mean age was 70 years, and 7 patients were female. 81 % of the skin reactions appeared after the 2nd dose. A mean delay between injection and symptom was 4.5 days after the 1st dose and 11.7 days after the 2nd. Skin lesions appeared on trunk ($n=8$), legs ($n=6$) and arms ($n=5$). Clinical patterns were erythematous ($n=6$), purpuric ($n=2$), urticarial ($n=1$), prurigo ($n=1$) and pityriasis rosea-like ($n=1$). Main histological pattern was drug reaction-like rash. We also observed pigmented purpuric dermatosis, perforating collagenosis, vasculitis and acantholytic dermatosis.
**Conclusion:** This study included only patients with skin biopsy. Biopsies were performed to help on the differential diagnosis and for the pharmacovigilance reporting. Even though the skin reactions are quite rare related to the number of vaccinations, it remains important not to misdiagnose a cutaneous reaction related to the vaccine. A proper clinicopathological classification will be helpful in the early diagnosis and management of these cutaneous reactions, and also give some clues about their physiopathological mechanisms.

## P 3
## Chaperone-mediated autophagy markers LAMP2A and HSPA8 in advanced non-small cell lung cancer after neoadjuvant therapy

Tereza Losmanova* [1], Philipp Zens[1], Mario Tschan[1], Amina Scherz[2], Ralph Schmid[2], Sabina Berezowska[3]

[1]University of Bern, Institute of Pathology, Bern, Switzerland [2]Inselspital University Hospital Bern, Bern, Switzerland [3]University of Lausanne, Institute of Pathology, Lausanne, Switzerland

In recent years autophagy has attracted the attention of researchers from many medical fields, including cancer research and certain anti-macroautophagy drugs in combination with cytotoxic or targeted therapies entered clinical trials. In the present study, we focused on a less explored subtype of autophagy–chaperone mediated autophagy (CMA), with the key players LAMP2A and HSPA8 (HSC70), and their immunohistochemical evaluation with previously extensively validated antibodies. We aimed to evaluate if marker expression is influenced by the antecedent therapy, and its correlation with survival in a cohort of patients with non-small cell lung cancer (NSCLC) resected after neoadjuvant therapy and matched primary resected tumors. In concordance with our previous study, we did not find any intratumoral heterogeneity, nor correlation between the two parameters, nor correlation between the markers and any included pathological parameters. Surprisingly, the expression of both markers was also independent to tumor response or administered neoadjuvant treatment. In the survival analysis, the results were only significant for LAMP2A, where higher levels were associated with better 5-year overall survival and disease free survival for the mixed group of adenocarcinomas and squamous cell carcinomas ($p < 0.0001$ and $p = 0.0019$ respectively) as well as the squamous cell carcinoma subgroup ($p = 0.0001$ and $p = 0.00099$ respectively). LAMP2A was also an independent prognostic marker in multivariate analysis.

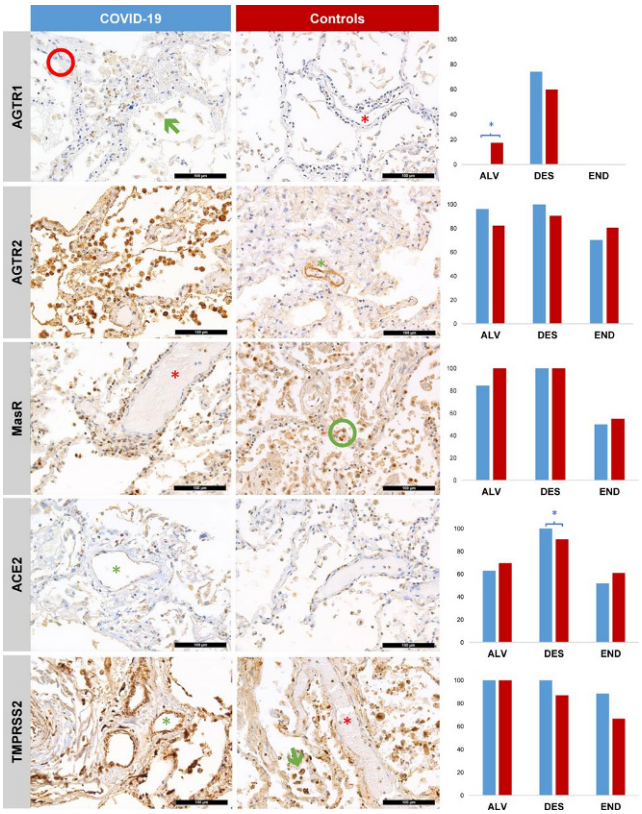


**Fig. 1 | P 4 ▲**

## P 4
## Analysis of SARS-CoV-2 entry factors and renin-angiotensin-aldosterone system components in lethal COVID-19

Jasmin Haslbauer* [1], Anna Stalder[1], Carl Zinner[2], Stefano Bassetti[3], Kirsten Mertz[4], Philip Went[5], Matthias Matter[1], Alexandar Tzankov[1]

[1]Pathology, Institute of Medical Genetics and Pathology, University Hospital Basel, University of Basel, Switzerland; [2]Institute of Biomedicine, University of Basel, Basel, Switzerland [3]Department of Internal Medicine, University Hospital Basel, University of Basel, Basel, Switzerland [4]Department of Pathology, Kantonsspital Baselland, Baselland, Switzerland [5]Department of Pathology, Kantonsspital Graubünden, Graubünden, Switzerland

**Background:** Since Angiotensin Converting Enzyme 2 (ACE2) was discovered as an essential entry factor of SARS-CoV-2, there has been conflicting evidence regarding the role of Renin-Angiotensin-Aldosterone System (RAAS) in COVID-19. This study elucidates pulmonary expression patterns SARS-CoV-2 entry-factors (ACE2 and Transmembrane Protease Serine Subtype 2, TMPRSS2) and RAAS-components in lethal COVID-19.
**Methods:** Lung tissue from COVID-19 autopsies ($n = 27$) and controls ($n = 23$) underwent immunohistochemical staining for RAAS-components (angiotensin receptors 1 and 2, AGTR1&2; ACE2 and Mas-receptor, MasR) and TMPRSS2. Staining of individual cellular populations (alveolar pneumocytes, ALV; desquamated cells, DES; endothelium, END) was measured by a binary scale (positive/negative). SARS-CoV-2 viral load was measured by qRT-PCR. Gene expression quantification for ACE2, ACE and TMPRSS2 was performed.
**Results:** Subtle differences were observed when comparing COVID-19 patients and controls not reaching statistical significance, such as a higher incidence of ACE2-positivity in END (52 % vs. 39 %) but lower positivity in ALV (63 % vs. 70 %) and an overall downregulation of ACE2 gene expres-

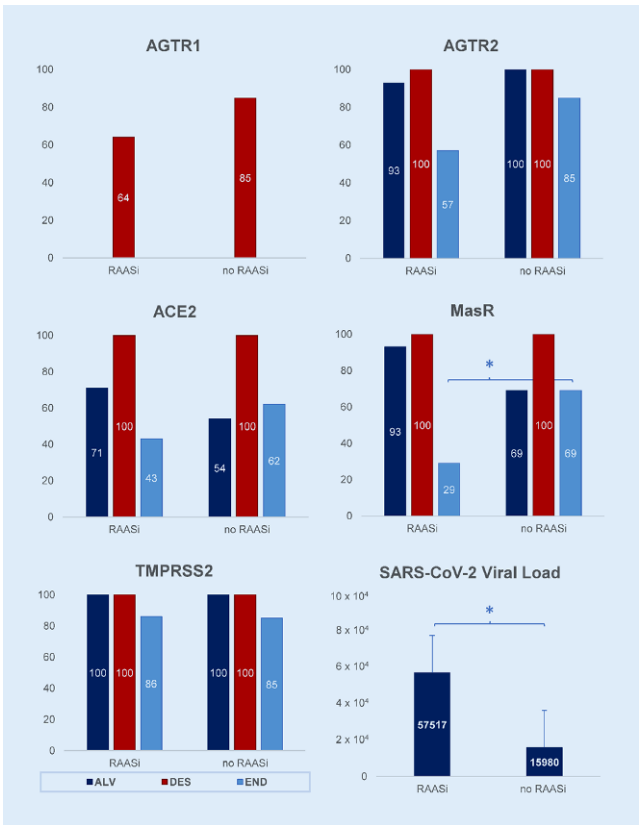


**Fig. 2 | P 4 ▲**

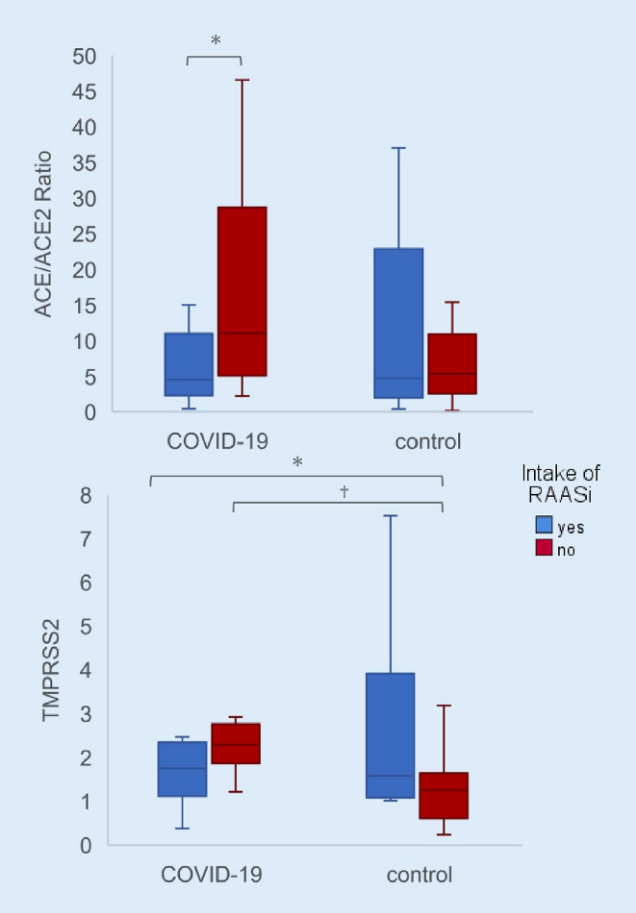


**Fig. 3 | P 4 ▲**

sion (2.2-fold) (**Fig. 1**). However, COVID-19 patients with RAAS-inhibitor (RAASi) intake had significantly shorter hospitalization times (5 vs. 12 days) and higher viral loads (57,517 vs. 15,980/106 RPPH1-copies) than patients without (**Fig. 2**). Furthermore, COVID-19 patients with RAASi intake showed decreased ACE/ACE2-expression ratios (4.58 vs. 11.07) and significantly higher overall TMPRSS2 expression (1.76-fold) in the COVID-19 cohort compared to controls (**Fig. 3**).

**Conclusion:** Our study delineates the heterogeneous expression patterns of RAAS-components in the lungs, which vary amongst cellular populations, and implies that COVID-19 patients with RAASi-intake present with a more rapid disease progression, although this requires further investigation.

## P 5
## Simplified molecular classification of gastric adenocarcinoma including lymph node status: an integrative approach towards a consensus classification

Ronny Nienhold* [1], Till Daun[1], Aino Paasinen-Sohns[2], Angela Frank[1], Melanie Sachs[1], Inti Zlobec[3],

Gieri Cathomas 1; [1]Kantonsspital Baselland, Baselland, Switzerland [2]Universität Basel, Basel, Switzerland [3]Universität Bern, Bern, Switzerland

**Background:** Gastric adenocarcinoma (GAC) is a heterogeneous disease and at least two major molecular classifications have been proposed. Both classifications quote four molecular sub-types, but these subtypes only partially overlap. In addition, the classifications are based on complex and cost-intensive technologies. Therefore, simplified approaches using commercially available tests and a consensus classification for the everyday practice are needed.

**Methods:** In a retrospective study, FFPE tissue of GAC was tested by immunohistochemistry (p53, MutL Homolog 1 (MLH1) and E-cadherin), in situ hybridization (EBV-EBER) and NGS (molecular analysis of tumor-associated genes including p53). The presence of lymph node metastasis and survival data were taken from the clinical charts.

**Results:** A total of 115 GAC were analyzed and grouped in five subtypes: (1) Microsatellite Instable (MSI), (2) EBVassociated, (3) Epithelial Mesenchymal Transition (EMT)-like, (4) p53 aberrant tumors surrogating for chromosomal in-stability and (5) p53 proficient tumors surrogating for genomics stable cancers. Furthermore, by considering lymph node metastasis in the p53 aberrant GAC, we were able to identify patients with poor and good-tointermediate prognosis.

**Conclusions:** Our data show that a simplified molecular classification of GAC can be achieved by using commercially available assays including IHC, ISH and NGS. Furthermore, we propose a consensus workflow, which, by integrating the presence of lymph node metastasis, show a high prognostic relevance.

## P 6
## Prognostic image-based quantification of CD8/CD103 T cell subset in high-grade serous ovarian cancer patients

Dominik Loiero* [1], Sterre T. Paijens[2], Annegé Vledder[2], Evelien W. Duiker[3], Joost Bart[3], Anne M. Hendriks[4], Mathilde Jalving[4], Hagma H. Workel[2], Harry Hollema[3], Annechien Plat[2], G. Bea A. Wisman[2], Refika Yigit[2], Henriëtte Arts[2], Arnold J. Kruse[5], Natascha M. de Lange[5], Marco de Bruyn[2], Hans W. Nijman[2], Viktor H. Kölzer[1]

[1]Department of Pathology and Molecular Pathology, University Hospital and University of Zurich, Zurich, Switzerland; [2]Department of Obstetrics and Gynecology, University of Groningen, University Medical Center Groningen, Groningen, The Netherlands; [3]Department of Pathology, University of Groningen, University Medical Center Groningen, Groningen, The Netherlands; [4]Department of Medical Oncology, University of Groningen, University Medical Center Groningen, Groningen, The Netherlands; [5]Department of Obstetrics and Gynecology, Isala Hospital Zwolle, Zwolle, The Netherlands

**Background:** CD103-positive tissue resident memory-like CD8+ T cells (CD8/CD103 TRM) are associated with improved prognosis across malignancies, including high-grade serous ovarian cancer (HGSOC). We investigated whether quantification of CD8, CD103 or both is required to improve existing survival prediction and whether all HGSOC patients or only specific subgroups of patients benefit from infiltration.

**Methods:** Tumor tissue of 268 Patients with advanced stage HGSOC from two independent clinics was stained with a CD8 and CD103 multiplex immunohistochemistry. The analysis of T-cell infiltrates in tumor and stroma compartments was carried out digitally using machine learning.

**Results:** Infiltration of CD8/CD103 immune cell subsets was independent of clinicopathological factors and previous neo-adjuvant chemotherapy. A survival benefit of epithelial and stromal CD8/CD103 TRM infiltration was observed in patients treated with primary cytoreductive surgery and no macroscopic tumor lesions after surgery (high epithelial CD8/CD103 TRM infiltration 5 year survival 83 % versus 52 %, $p = 0.03$; high stromal CD8/CD103 TRM 5 year survival 77 % versus 54 %, $p = 0.01$). Neither single CD8 positive cells (HR 1.02 [0.92–1.1], $p = 0.76$) nor single CD103 positive cells (HR 0.92 [0.80–1.1], $p = 0.23$) were associated with improved outcome. No effect of CD8/CD103 TRM infiltration on overall survival was observed in patients treated with neoadjuvant chemotherapy, with or without macroscopic tumor lesions after surgery (high epithelial CD8/CD103 TRM infiltration, $p = 0.77$; high stromal CD8/CD103 TRM infiltration, $p = 0.32$).

**Conclusion:** Our results suggest CD8/CD103 TRM quantification as a superior method for prognostication compared to single CD8 or CD103 quantification, and advocates the further exploration of image-based quantification of CD8/CD103 TRM in HGSOC. This approach provides novel insights into prognostic stratification of HGSOC patients and may contribute to personalized treatment strategies in the future.

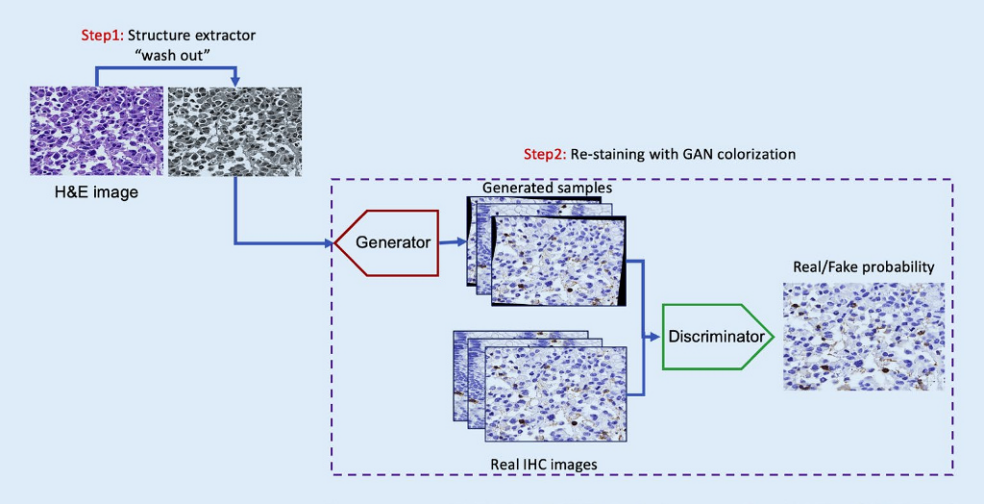


**Fig. 1 | P 8** ◀

## P 7
## AI-aided assessment of HER2-Status in invasive breast cancer*

Christiane Palm*, Annina Fasler, Konstantinos Koutsospyros, Marianne Tinguely

Pathologie Institut Enge, Zurich, Switzerland

**Background:** Determination of HER2 status in breast cancer patients is critical to decide on the appropriate therapy. Inter-observer variability of HER2 IHC scoring by pathologists can affect diagnostic accuracy. The aim of our study was to determine the feasibility of artificial intelligence (AI) assisted scoring of HER2 IHC and ISH on digitalized slides.
**Methods:** We digitalized 476 core-needle-biopsies (CNB) of invasive breast cancers (VENTANA DP200 slide scanner, Roche) and determined the HER2 IHC score with the upath HER2 4B5 AI software. We compared the results of our tissue adapted in-house protocol with a test cohort of 19 cases applying the package-insert protocol (both HER2 IHC pathway test Ventana Roche (Clone 4B5)). Additionally, 71/476 cases were analyzed by ISH (upath HER2 Dual ISH, Ventana Roche). We compared the pathologist's performance with the one of the automated algorithm.
**Results:** Concordance of AI with pathologists was higher in the 19 cases analyzed by the package-insert protocol (13/19; 68.42 %) than among those using the house-intern protocol (182/476; 38.24 %). Out of the six (31.58 %) discordant cases stained with the package-insert protocol, four (21.05 %) were without and two (10.53 %) entailed clinical consequences. The AI's scoring of 71 ISH slides exhibited concordance in 62 (87.32 %) after manual editing. All nine discordant ISH cases (12.68 %) were interpreted as equivocal, in eight cases by AI and in one by a pathologist.
Altogether, concordance rates between AI and different pathologists ranged from 25.95–54.0 % in IHC and from 80.0–100 % in ISH.
**Conclusion:** Tight adherence to package-insert staining protocol is mandatory to receive optimal AI results for IHC. While the scoring accuracy is higher in ISH than in IHC, extensive manual editing of the AI's ISH scoring process is needed. Although AI-aided scoring suggests minimizing inter-pathologist scoring variability, further developments in their applicability for diagnostic use is necessary.
*Student paper

## P 8
## Generation of virtual CD20-CD3 staining from H&E images using deep learning

Huu Giao Nguyen* [1], Jose A. Galvan[1], Heather Dawson[1], Alessandro Lugli[1], Inti Zlobec[2]

[1]Institute of Pathology, University of Bern, Bern, Switzerland [2]Universität Bern, Bern, Switzerland

**Background:** CD20 and CD3 are commonly used as specific markers of B- and T-Lymphocytes, respectively, and help identify and quantify tumor-infiltrating lymphocytes (TIL). The quantification of lymphocytes on H&E stains, however, can be challenging for both human observers and machine learning algorithms. The aim of this study is to automatically generate CD20-CD3 double stained images from corresponding H&E stains using a generative adversarial network (GAN) colorization method.
**Data and method:** A training dataset with 34790 H&E images (size 384 × 256 pixels) and its corresponding CD20-CD3 images obtained after re-staining from 703 TMA spots of 295 patients was considered. From an input H&E image, we apply a tissue structure extractor method (wash-out the color of H&E) and two neural networks for generator and discriminator to learn the CD20-CD3 colorization (re-stain). The method and colorization examples are visualized in **Fig. 1 and 2**, respectively.
**Measurement tool and results:** For the TIL quantification, the bounding box of the brown (B-cell) and red (T-cell) objects in generated images was detected and extracted. Afterwards, the Intersection over Union (IoU) score which essentially quantifies the percent overlap between the target mask and our prediction output was estimated (**Fig. 3**). Based on a validation set of 3150 H&E images, a high correlation between real and generated images was obtained (IoU score = 91.3 %).
**Conclusions:** The present study proposes a potential effective computational method from H&E data to generate different immunohistochemis-

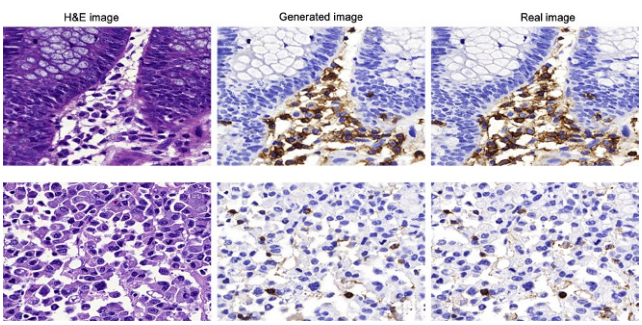


**Fig. 2 | P 8** ▲

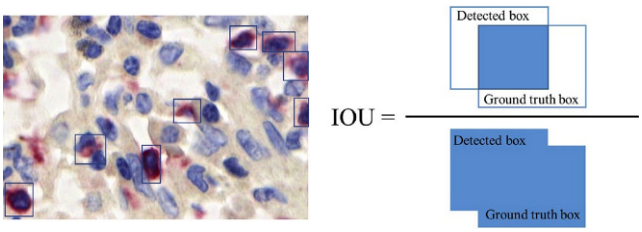


**Fig. 3 | P 8** ▲

try staining avoiding a standard lab workflow. Therefore, a full application for quantification of TIL with lymphocytes detection and epithelium segmentation is being developed.

## P 9
## Reducing the annotation workload: using self-supervised methods to learn from public available colorectal cancer datasets

Christian Abbet*

Signal Processing Lab 5 (LTS5), EPFL, Lausanne, Switzerland

**Background:** Supervised learning is constrained by the availability of labeled data, which are especially expensive to acquire as they are very time-consuming and need expert knowledge. Making use of open-source data and applying domain adaptation can be a way to overcome this issue. Combining this with self-supervised learning, where "the data creates its own supervision" allows us to learn rich features from unlabeled data. We apply this method to tissue type detection, which is helpful for many downstream tasks such as the prediction of prognostic factors.
**Methods:** We use our proposed Self-Rule to Adapt (SRA) framework [1] to perform self-supervised domain adaptation between an open-source colorectal cancer dataset [2] and our in-house H&E-stained adenocarcinoma cohort. The method learns the representation of the data using an easy-to-hard approach where it starts to learn from tissues with low visual complexity and then slowly moves toward more challenging examples as it becomes more robust.
**Results:** To assess the quality of our model, we use selected tissue regions from our in-house cohort where annotations were made available. We compare our results with the standard supervised transfer-learning baseline in terms of accuracy, weighted intersection or union, and pixel-wise Cohen's kappa score. The proposed method achieves 0.682, 0.548, 0.587 against 0.514, 0.408, 0.417 for the baseline over the previously introduced metrics.
**Conclusion:** We show that our proposed architecture is able to learn and classify complex tissue representation with few annotations, thus relieving the pathologist from tedious annotation work. As a result, it makes it a good candidate for future clinical applications where we rely on large sets of weakly labeled scans.

## References

1. https://openreview.net/forum?id=VO7asaS5GUk
2. https://zenodo.org/record/1214456

## P 10
## Cell-based graphs for tissue classification in colorectal histopathology images*

Ana Frei* [1], Christian Abbet[2], Inti Zlobec[3], Jean-Philippe Thiran[2]

[1]Institute of Pathology, University of Bern, Bern, Switzerland; [2]Signal Processing Lab 5 (LTS5), EPFL, Lausanne, Switzerland [3]Universität Bern, Bern, Switzerland

**Background:** Colorectal cancer (CRC) is highly heterogenous and composed of a variety of tissues. Different types of cells compose these tissues, forming the tumor microenvironment (TME). Cells are not randomly located in the tissues but organized into structured patterns to perform specific functions. Cell-based graphs can model structurefunction association. Here, we aim to classify tiles from CRC whole slide images (WSI) into their corresponding tissue type using this graph approach.
**Methods:** CRC WSIs are cropped into smaller patches on which cells are detected and classified into multiple cell types. Cell-based graphs are built as follows: cells are the nodes of the graphs and edges are the connections between the cells. Delaunay triangulation is used to determine the edges between the closest neighbors of each cell in the image. A threshold is used to prevent connections between distant cells that are unlikely to communicate with each other. Graphs are then classified using Graph convolutional Networks (GCNs).
**Results:** A segmentation from the input image is obtained upon graph classification. The model achieves a classification accuracy (F1-score) above 85 % on Kather19 dataset [1]. When using tiles from WSI from the Institute of Pathology of Bern, the output segmentation is representative of the tissue types present in the slide and the global structure and organization of the tissues are similar to pathologist's annotations, demonstrating that the model is working.
**Conclusion:** With this method, it was possible to classify CRC tissues into 6 classes with an accuracy above 85 % on Kather19 dataset. This demonstrates that cell-based graphs are powerful representations of tissue structures, compositions and cell-cell interaction that are related to tissue function.
*Student paper

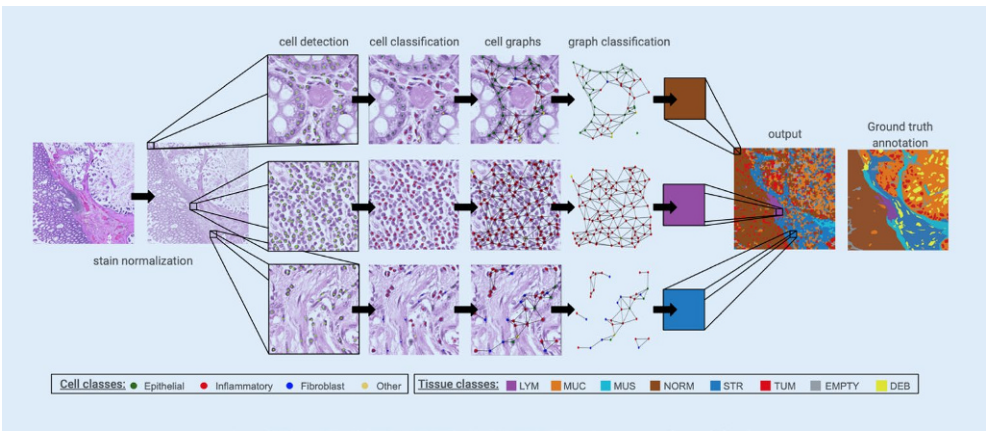


**Fig. 1 | P 10** ◀ Patch classification pipeline. First the histology images are normalized. Then, for each patch, cells are detected and classified into four cell classes (epithelial, inflammatory, fibroblast, other). Cell-based graphs are built using the cells as nodes and adjacent nodes are connected by edges. Finally, the graphs are classified into seven classes (lymphocytes, mucus, muscle, normal, stroma, tumor and empty), resulting in the segmentation of the initial image

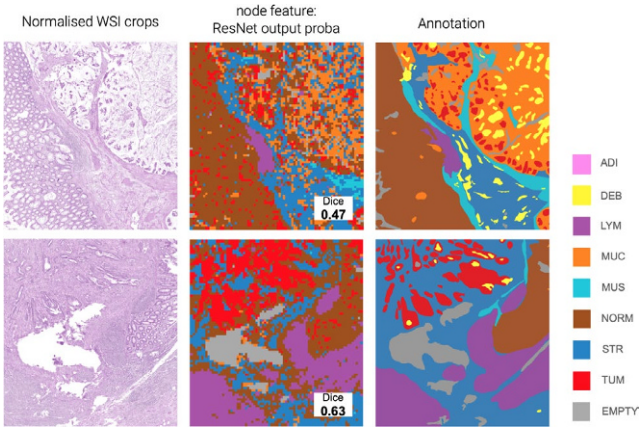


**Fig. 2 | P 10** ▲ Tissue classification output on WSI crops. The model was applied on two crops from different WSI. The input image was colored based on the patch classification output. Each tissue type is represented by a specific color. The first column represents the normalized input crops, the second column the output from the model and the third column the ground truth annotations by pathologists. DICE scores for each crop are highlighted in white

| | LYM | MUC | MUS | NORM | STR | TUM | Avg. F1 |
|---|---|---|---|---|---|---|---|
| DGCNN onehot labels | 0.97 | 0.69 | 0.78 | 0.70 | 0.70 | 0.81 | 0.77 ± 0.006 |
| GraphSAGE onehot labels | 0.97 | 0.64 | 0.77 | 0.74 | 0.70 | 0.79 | 0.77 ± 0.0074 |
| DGCNN proba labels | 0.99 | **0.80** | 0.82 | 0.84 | **0.81** | 0.85 | 0.85 ± 0.0051 |
| GraphSAGE proba labels | 0.99 | 0.79 | **0.86** | 0.84 | 0.80 | **0.86** | **0.86** ± 0.0084 |

**Fig. 3 | P 10** ▲ Classification performance of different GDNs on KAther19 dataset. F1 score was computed for each class as well as the average F1 score of each model

## References

1. Dataset consisting of 100'000 H&E stained colorectal histology images (224 × 224 pixels at 0.5 µm/pixel) divided into their corresponding tissue classes (https://zenodo.org/record/1214456#.YTCFiS1PgWo).

## P 11
## The KRAS mutational status may predict the efficacy of immune checkpoint inhibitors in non-small cell lung cancer patients showing PD-L1 overexpression (TPS≥50 %)

Samantha Epistolio* [1], Marco Cefalì[2], Giulia Ramelli[1], Dylan Mangan[2], Francesca Molinari[1], Alexandra Valera[1], Vittoria Martin[1], Stefania Freguia[3], Luca Mazzucchelli[3], Luciano Wannesson[2], Milo Frattini[1]

[1]Laboratory of Molecular Pathology, Institute of Pathology, ICP, EOC, Locarno, Switzerland [2]Oncology Institute of Southern Switzerland, IOSI, EOC, Bellinzona, Switerland [3]Institute of Pathology, ICP, EOC, Locarno, Switzerland

**Background:** Immune checkpoint inhibitors (ICIs) targeting programmed cell death protein 1/programmed cell death-ligand 1 (PD-1/PD-L1) have contributed to improve the survival of lung adenocarcinoma (AC) with PD-L1 expression and without mutations in EGFR or translocations in ALK, ROS1, RET genes. However, markers able to predict the efficacy of ICIs, in combination with PD-L1 expression, are still lacking. Our aim was to evaluate whether KRAS mutations, may predict the efficacy of ICIs in stage IV lung AC patients.
**Methods:** We retrospectively retrieved 81 stage IV lung AC treated in first-line with ICIs and with PD-L1 overexpression (TPS≥50 %). From these we selected 44 patients harbouring KRAS mutation but no EGFR, ALK, ROS1 or RET genetic alterations. Formalin-fixed paraffin embedded samples were tested using Next Generation Sequencing (EGFR and KRAS point mutations/small indels, through Ion Torrent technology), Fluorescence in Situ Hybridization (ALK, ROS1 and RET gene fusions), and immunohistochemistry (PD-L1 protein expression, SP263 clone). Statistical analyses were done applying the log rank test and the Kaplan-Maier plot.
**Results:** KRAS G12C mutated patients ($n = 11/44$) are characterized by a better survival, in particular by a longer progression free survival (PFS) ($p = 0.03$) but not by a different overall survival (OS) ($p = 0.47$). The Kaplan-Maier plot of the PFS time to events supports that G12C positive patients have a longer time to progression of disease or death.
**Conclusions:** The KRAS G12C mutation can be considered a predictive marker of good response to first line ICIs in lung AC patients overexpressing PD-L1 and not carrying alterations in EGFR, ALK, ROS1 and RET. This finding could be relevant when anti-KRAS G12C therapies will be available.

## P 12
## Anthracosis–a pitfall for accurate nuclei segmentation in lung tissue*

Philipp Zens* [1], Sabina Berezowska[2]

[1]University of Bern, Institute of Pathology, Bern, Switzerland [2]University of Lausanne, Institute of Pathology, Lausanne, Switzerland

Nuclei detection is a basic task of artificial intelligence (AI)-based algorithms applied in pathology. There is a plethora of techniques available for automatic nuclei detection. However, all these techniques are error-prone when applied to routine lung tissue slides because of an organ specific artefact: anthracosis. We approached the problem of anthracosis twofold by training a neural network or applying watershed detection and adding an anthracosis classifier.
For the approach with watershed detection, we used 100 CD8 stained sections of non-small cell lung cancer cases, subsequently divided in 60 training and 40 testing images. For training, positive/negative cells and anthracosis were annotated after initial segmentation to train a classifier. For validation 5000 × 5000 pixels tiles were annotated and the performance was assessed regarding sensitivity and specificity. For the neural network approach, we generated a private dataset including 24 1000 × 1000 pixels tiles of CD8 stained sections from 2 patients with lung adenocarcinoma and 4 patients with lung squamous cell carcinoma. Eighteen tiles were used for training and 6 for testing. We trained the StarDist2D model using Intersection of Union as accuracy measure and assessed the performance in the test set using Dice score. Our anthracosis classifier yielded a mean sensitivity of 95 % and a mean specificity of 86 %. This approach allowed good identification of anthracosis and the removal of these false positive detections before further downstream analyses.

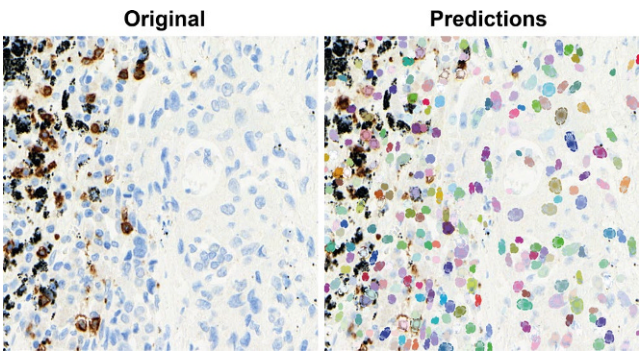


**Fig. 1 | P 12** ▲ Original image and predicted nuclei of the trained model. The dots represent the centroid of the prediction and the rays the radii to the boundary

Our network approach yielded in a dice score of 73 % when defining 70 % overlap with the ground truth as true positive nuclei. Importantly, qualitative assessment showed no false detection of anthracosis as nuclei making an anthracosis classifier needless.
Anthracosis is a ubiquitous problem for image analysis algorithms applied on lung tissue and hampers accurate automatic nuclei detection. We demonstrate that it is necessary and feasible to account for anthracosis in AI-based approaches for lung tissue.
*Student paper

## P 13
## Loss of MTAP expression by IHC is a surrogate marker for homozygous 9p21 deletion in urothelial carcinoma

Tatjana Vlajnic* [1], Obinna Chijioke[1], Serenella Eppenberger-Castori[1], Luca Roma[1], Tobias Zellweger[2], Cyrill A. Rentsch[3], Lukas Bubendorf[4]

[1]Institute of Medical Genetics and Pathology, University Hospital Basel, University of Basel, Basel, Switzerland; [2]Division of Urology, St. Clara Hospital, Basel, Switzerland; [3]University Hospital Basel, Department of Urology, Basel, Switzerland [4]University Hospital Basel, Institute of Medical Genetics and Pathology, Basel, Switzerland

**Background:** Homozygous deletion of the tumor suppressor gene CDKN2A (p16) is common in urothelial carcinoma (UC). MTAP (methylthioadenosine phosphorylase), a gene located next to CDKN2A on chromosome 9p21, is often codeleted, resulting in loss of MTAP protein expression. Fluorescence in situ hybridization (FISH) is regarded as the gold standard for detection of 9p21 deletion to clarify cases of inconclusive urothelial atypia. Here, we aimed at exploring the diagnostic potential of MTAP immunohistochemistry (IHC) as a surrogate marker for homozygous 9p21 deletion (hDel9p21) in UC.
**Material and Methods:** MTAP status was determined by IHC (2G4, Abnova) on 27 UC tissue specimens with known 9p21 status as defined by FISH in matched cytological specimens, by IHC and FISH on a TMA containing 176 non-muscle-invasive, 102 muscle-invasive and 32 metastatic UC specimens, and by IHC on 204 consecutive UC tissue specimens from routine practice. Moreover, we analyzed a longitudinal series of specimens from 14 patients with MTAP negative recurrent UC.
**Results:** In the matched cohort, MTAP loss by IHC was found in 16/17 cases with homozygous deletion and in 2/8 cases without 9p21 deletion (sensitivity 94 %, specificity 80 %). In the TMA, MTAP loss tended to be more common in muscle-invasive (56 %) than in non-muscle-invasive UC (42 %) and was significantly more common in metastases (89 %) ($p < 0.01$). In the consecutive series, 43/204 (21 %) cases showed loss of MTAP expression. Interestingly, 15/43 cases (35 %) revealed heterogeneous MTAP loss in morphologically indistinguishable areas. Longitudinal analysis of MTAP negative recurrences showed persistent negative MTAP status over time in all 14 patients (mean time between resections: 35 months).
**Conclusion:** MTAP IHC can serve as a surrogate marker for homozygous 9p21 deletion in UC tissue specimens. Moreover, it provides a unique opportunity to study molecular heterogeneity of homozygous 9p21 deletion.

## P 14
## PD-L1 expression in digestive neuroendocrine neoplasms (NENs): correlation with tumor immune microenvironment and clinico-pathologic features

Eleonore Multone* [1], Cindy Verasolis[1], Christine Sempoux[1], Fausto Sessa[2], Silvia Uccella[2], Stefano La Rosa[1]

[1]Lausanne University Hospital and University of Lausanne, Institute of Pathology, Department of Laboratory Medicine and Pathology, Lausanne, Switzerland [2]University of Insubria, Unit of Pathology, Department of Surgical and Morphological Sciences, Varese, Italy

**Background:** Digestive NENs are heterogeneous, encompassing a wide spectrum of neoplasms ranging from indolent well-differentiated neuroendocrine tumors (NETs) to highly aggressive neuroendocrine carcinomas (NECs). The PD-1/PD-L1 pathway plays a pivotal role in T cells activation and host immune response to cancer. PD-L1 expression in tumor and/or immune cells has been suggested as a prognostic biomarker in different type of cancers, allowing the identification of patients who can be treated with targeted checkpoint inhibitors. However, the prognostic role of PD-L1 expression in digestive NENs is still unclear.
**Methods:** We investigated PD-L1 expression using the SP263 antibody (Ventana Medical System) in 68 wellcharacterized digestive NENs: 32 NETs and 36 NECs. TPS and CPS PD-L1 scores, tumor infiltrating lymphocytes (using the anti-CD3, CD4, and CD8 antibodies), and mismatch repair (MMR) protein expression (quantitatively, using the anti-hMLH1, hPMS2, hMSH6, and hPMS2 antibodies) were evaluated. Immunohistochemical findings were correlated with clinicopathological data.
**Results:** PD-L1 scores TPS >1 % and/or CPS >1 were observed in 5/32 NETs and 23/36 NECs (p: 0.05). The mean TPS score in positive cases was 6.3 % and 14 % in NETs and NECs, respectively and the CPS score was 4.8 and 7.91, respectively. MMR-deficient neoplasms were more frequently observed in NECs than in NETs (2 NETs and 5 NECs, p: <0.05). No correlation between PD-L1 expression and survival or other clinico-pathological parameters was found, including Ki67-proliferative index and MMR-deficiency. Intra-tumor immune infiltration was statistically more abundant in NECs than in NETs.
**Conclusions:** The heterogeneous expression of PD-L1 in NENs, with only a few positive cases among NETs, seems to indicate that targeted checkpoint inhibitors therapy may have a potential role only in selected cases, mainly in NECs. T-cell infiltrate is more abundant in NECs than in NETs, supporting the possible application of immunological therapy in NECs.

## P 15
## Immunohistochemical H3K27 m3 expression–a promising tool in the differential diagnosis between reactive follicular hyperplasia and follicular lymphoma

Magdalena M. Brune* [1], Stefan Dirnhofer[1], Visar Vela[1], Alexandar Tzankov[2]

[1]Institute of Medical Genetics and Pathology, University Hospital Basel; [2]Pathology, Institute of Medical Genetics and Pathology, University Hospital Basel, University of Basel, Switzerland

**Background:** To differentiate reactive follicular hyperplasia (FH) from follicular lymphoma (FL), which bears substantial consequences for the patient, can be a challenging task in daily routine. Immunohistochemical (IHC) staining for BCL2–a surrogate marker for FL's hallmark translocation t(14;18)–or fluorescent in situ-hybridization (FISH) for BCL2 to address the presence of rearrangements, are helpful in many, but not all cases, since 10–15 % of FL are negative for either protein and/or rearrangement. Next to t(14;18), genetic alterations in epigenetic regulatorencoding genes are identified in almost all FL, leading, among others, to recurrent trimethylation of histone H3 at the position lysine 27 (H3K27). This condition can be visualized by an antibody against trimethylated H3K27 (H3K27 m3). In this study, we investigated whether the diagnostic use of IHC for H3K27 m3 is

suitable to distinguish FH from FL and adds value compared to BCL2 IHC staining and/or FISH.
**Methods:** We investigated the IHC expression of H3K27 m3 in 39 cases of FH (lymph nodes and tonsils) and in 129 cases of FL (conventional and tissue-microarrayed samples) of all grades, both (IHC and/or FISH) BCL2-positive and BCL2-negative. In 10 cases results were correlated with the known EZH2mutational status.
**Results:** 114/129 (88 %) FL displayed a moderate to strong expression of H3K27 m3 in the neoplastic germinal centers, whereas only 1/39 (3 %) FH showed moderate expression in germinal centers (p2-sided Fisher's exact test<0.0001). The expression of H3K27 m3 in FL did neither correlate with IHC expression of BCL2 (SP66 and E17 antibody) nor with the presence of FISH-detectable BCL2 gene rearrangements, and occurred independently of EZH2 mutations.
**Conclusion:** Determination of the IHC expression of H3K27 m3 is a helpful tool in the differential diagnosis between FH and FL that may be of added value in particular in BCL2-negative FL, as H3K27's trimethylation occurs independently of the BCL2-status.

## P 16
## An exploratory analysis of the association between HSD3B1 gene polymorphisms and outcomes in SARS-CoV-2 infected patients

Giulia Ramelli* [1], Ricardo Pereira Mestre[2], Samantha Epistolio[1], Margaret Ottaviano[2], Emanuele Crupi[2], Laura Marandino[2], Maira Biggiogero[3], Pier Andrea Maida[3], Lorenzo Ruinelli[4], Ursula Vogl[2], Dylan Mangan[2], Mariarosa Pascale[5], Marco Cantù[6], Alessandro Ceschi[7], Federico Mattia Stefanini[8], Enos Bernasconi[9], Luca Mazzucchelli[10], Carlo Catapano[11], Andrea Alimonti[11], Christian Garzoni[3], Alessandra Franzetti Pellanda[3], Silke Gillessen Sommer[2], Milo Frattini[1]

[1]Laboratory of Molecular Pathology, Institute of Pathology, ICP, EOC, Locarno, Switzerland [2]Oncology Institute of Southern Switzerland (IOSI), EOC, Bellinzona, Switzerland [3]Clinic of Internal Medicine and Infectious Diseases, Clinica Luganese Moncucco, Lugano, Switzerland [4]ICT, Informatica e Tecnologia della Comunicazione, EOC, Bellinzona, Switzerland [5]Clinical Trial Unit, EOC, Lugano, Switzerland [6]EOLAB, EOC, Bellinzona, Switzerland [7]Division of Clinical Pharmacology and Toxicology, Institute of Pharmacological Sciences of Southern Switzerland, EOC, Lugano, Switzerland [8]Faculty of Science and Technology–ESP, University of Milan, Milano, Italy [9]Department of Medicine, Division of Infectious Diseases, EOC, Lugano, Switzerland 1[0]Institute of Pathology, ICP, EOC, Locarno, Switzerland 1[1]Institute of Oncology Research (IOR), Università della Svizzera italiana (USI), Bellinzona, Switzerland

**Background:** Early evidence suggests that SARS-CoV-2 uses the Androgen Receptor (AR) pathway, through ACE2 receptor and TMPRSS2, to enter nasal and upper airways epithelial cells. Many clinical parameters have been associated with SARS-CoV-2 infection severity, but to date no definitive genetic data exist to support androgen-mediated viral infection. In the AR pathway, genetic analysis revealed that HSD3B1 1245CC polymorphic variant increases dihydrotestosterone production and upregulation of TMPRSS2 with respect to 1245AA variant. Our aim was to characterize the HSD3B1 polymorphism status in hospitalized SARS-CoV-2 patients in Ticino.
**Methods:** Study population consisted of 400 patients hospitalized during the first wave between February and May 2020. Genomic DNA was extracted from six 4 µm-thick sections of formalin-fixed paraffin-embedded tissue blocks using a standard protocol starting from any material available in our archives. HSD3B1 gene polymorphism was evaluated by Sanger sequencing. Statistical hypotheses were tested by Kruskal-Wallis rank sum test, asymptotic Wilcoxon-Mann-Whitney Test, Mood two-sample test of scale, asymptotic Two-Sample Fisher-Pitman Permutation Test. Generalized Linear models were fitted using the R software.
**Results:** The presence of co-morbidity such as hypertension, cardiovascular disease, diabetes and tumor were significantly associated with increased risk of death in the overall population. The HSD3B1 polymorphism status was significantly associated with sex and diabetes influencing admission to intensive care. A similar significant association was observed for HSD3B1 gene status and hypertension or age or presence of a tumor with respect to death from infection.
**Conclusions:** This is the first study showing that HSD3B1 gene status may influence the severity of SARS-CoV-2 infection. We report that HSD3B1 variants may play a clinical role in specific subgroups of patients affected by SARS-CoV-2, based on sex and co-morbidities. If confirmed, our results could lead to the introduction of HSD3B1 gene status analysis in SARS-CoV-2 infected patients in order to predict clinical outcome.

## P 17
## Solid pseudopapillary neoplasm of the pancreas with a non-CTNNB1 mutation in familial adenomatous polyposis–about a case and review of the literature

Alina Lungu* [1], Amedeo Sciarra[1], Igor Letovanec[1], Ian Fournier[2], Charles Bénière[1]

[1]Central Institute, Valais Hospital, Department of Histopathology, Sion, Switzerland [2]Valais Hospital, Department of Surgery, Sion, Switzerland

**Background:** Solid pseudopapillary neoplasms of the pancreas (SPN) develop mostly in young women and harbor a recurrent CTNNB1 (β-catenin) mutation. There are few reports of SPN in patients with Familial Adenomatous Polyposis (FAP), an inherited condition associated with a variety of gastro-intestinal and extra-intestinal lesions.
**Methods:** We present a case of a 38-years-old male patient, with a documented family history of FAP, presenting a pancreatic tumor, investigated by imaging (abdominal computed tomography and endoscopic ultrasound). Patient underwent genetic counselling. Histopathological analysis was performed on a fine needle aspiration biopsy, and included immunohistochemistry and targeted deep sequencing (26-gene panel).
**Results:** The genetic counselling identified APC p.E893* germinal mutation. Abdominal CT revealed a 4 cm welldemarcated mass in distal pancreas. Histologically, the tumor showed peritheliomatous pattern and pseudopapillae with monomorphous, polygonal cells, with an eosinophilic cytoplasm and round nuclei. Immunohistochemically, the tumor cells expressed β-catenin, E-cadherin, CD10, BCL-1, Sox-11 and progesterone receptors. Neuroendocrine markers (Synaptophysin, Chromogranin-A) were negative. The CTNNB1 gene profile was wildtype.
**Conclusion:** To our knowledge, this is the first case of a SPN in a male patient with FAP, without CTNNB1 mutation. Genetic studies have shown

**Fig. 1 | P 17** ▲ Computed tomography (CT) imaging of the pancreatic tumor. CT scan revealed a solid tumor of the caudal pancreas (arrow)

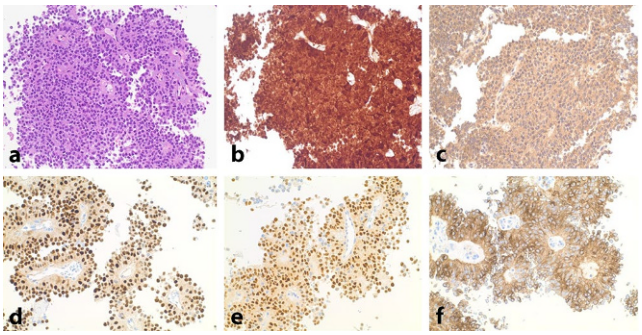


**Fig. 2 | P 17** ▲ Morphology and immunophenotype of the pancreatic tumor. a H&E pseudopapillary pattern. b β-catenin expression. c E-cadherin expression. d BCL-1 expression. e Progesterone receptors expression. f CD10 expression

that the pathological activation of the Wnt/β-catenin pathway, induced by the APC mutation, leads to the upregulation of Notch, Hedgehog and androgen receptor signaling pathways in FAP-associated tumors. Non-CTNNB1 dependent activation of the Wnt/β-catenin pathway suggests that the development of SPN in FAP patients may be APC driven, making it an entity belonging to the wide spectrum of tumors seen in FAP.

## P 18
## Mcl1ΔIEC mice: a pre-clinical model of intestinal apoptosis revealing new insights into apoptotic enteropathy and intestinal carcinogenesis

Marc Healy* [1], Yannick Boege[2], Michael Hodder[3], Friederike Böhm[4], Mohsen Malehmir[5], Anna-Lena Scherr[6], Jasna Jetzer[4], Lap Kwan Chan[4], Rossella Parrotta[4], Mercedes Gomez de Agüero[7], Kristian Unger[8], Andrew Macpherson[7], Andreas Moor[9], Bruno Köhler[6], Owen Sansom[3], Mathias Heikenwalder[10], Achim Weber[1]

[1]Department of Pathology and Molecular Pathology, University Hospital Zurich, Zurich; Institute of Molecular Cancer Research, University of Zurich, Zurich, Switzerland [2]Department of Pathology and Molecular Pathology, University Hospital Zurich, Zurich, Switzerland [3]Cancer Research UK Beatson Institute, Garscube Estate, Bearsden, Glasgow, UK [4]Department of Pathology and Molecular Pathology, University Hospital and University of Zurich, Zurich, Switzerland; [5]Department of Pathology, Zurich, Switzerland [6]National Center for Tumor Diseases, Department of Medical Oncology and Heidelberg University Hospital, Internal Medicine VI, Heidelberg, Germany [7]Maurice Müller Laboratories (DKF), Universitätsklinik für Viszerale Chirurgie und Medizin Inselspital, University of Bern, Bern, Switzerland [8]Research Unit of Radiation Cytogenetics, Helmholtz Zentrum München, Neuherberg, Germany [9]Institute of Molecular Cancer Research, University of Zurich, Zurich, Switzerland 1[9]Division of Chronic Inflammation and Cancer, Deutsches Krebs-Forschungszentrum (DKFZ), Heidelberg, Germany

**Background:** 'Apoptotic enteropathy' refers to a colitis-like pattern of gastrointestinal injury with intestinal epithelial cell (IEC) apoptosis being the hallmark of disease. While apoptotic enteropathy has long been observed as a feature of Graft-versus Host-Disease (GvHD) or viral infection, recent clinical findings have highlighted the emergence of apoptotic enteropathy as a result from drug-induced injury.
**Methods:** We have created a pre-clinical model of apoptotic enteropathy by generating mice with IEC-specific disruption of Mcl1 (Mcl1DIEC mice). These mice and littermate controls were raised under normal or germ-free conditions. Mice were examined endoscopically, calprotectin levels were measured as a marker of intestinal inflammation, and intestinal epithelial barrier permeability was also determined. Intestinal tissues were analysed by histology, immunohistochemistry, in situ hybridisation, immunoblots, gene expression and mutational profiling.
**Results:** Mcl1DIEC mice spontaneously developed apoptotic enteropathy characterized by diarrhoea, increased IEC apoptosis, hyperproliferative crypts, epithelial barrier dysfunction and chronic inflammation. Loss of MCL1 retained intestinal stem cells (ISC) in a hyperproliferative state and prevented differentiation. Proliferation of ISC in MCL1-deficient mice was WNT signaling-dependent and associated with accumulation of DNA damage. Aged Mcl1DIEC mice developed intestinal tumors with morphological and genetic features of human colorectal adenomas and carcinomas. Germ-free housing of Mcl1DIEC mice eliminated microbiota-induced intestinal inflammation, but not tumor development.
**Conclusion:** The anti-apoptotic BCL2 family member MCL1 is essential for maintaining intestinal homeostasis and preventing carcinogenesis. Loss of MCL1 leads to the development of intestinal carcinomas even under germ-free conditions, thus occurs independently of microbiota-induced chronic inflammation. Our results demonstrate that persistently increased apoptosis of IEC may be the trigger of WNT signaling-driven bowel cancer development. These observations have implications not only for understanding intestinal carcinogenesis but also drug-induced apoptotic enteropathy.

## P 19
## What's behind 68Ga-PSMA-11 uptake in primary prostate cancer PET? Investigation of histopathological parameters and immunohistochemical PSMA expression patterns

Jan H. Rüschoff* [1], Daniela A. Ferraro[2], Urs J. Muehlematter[2], Riccardo Laudicella[2], Thomas Hermanns[3], AnnKatrin Rodewald[4], Holger Moch[4], Daniel Eberli[3], Irene A. Burger[2], Niels J. Rupp[4]

[1]Department of Pathology and Molecular Pathology, University Hospital Zurich, Zurich, Switzerland [2]Department of Nuclear Medicine, University Hospital Zurich, University of Zurich, Zurich, Switzerland [3]Department of Urology, University Hospital Zurich, University of Zurich, Zurich, Switzerland [4]Department of Pathology and Molecular Pathology, University Hospital Zurich, University of Zurich, Zurich, Switzerland

**Purpose:** Prostate-specific membrane antigen (PSMA-)PET has become a promising tool in staging and restaging of prostate carcinoma (PCa). However, specific primary tumour features might impact accuracy of PSMA-PET for PCa detection. We investigated histopathological parameters and immunohistochemical PSMA expression patterns on radical prostatectomy (RPE) specimens and correlated them to the corresponding 68Ga-PSMA-11-PET examinations.
**Methods:** RPE specimens of 62 patients with preoperative 68Ga-PSMA-11-PET between 2016 and 2018 were analysed. WHO/ISUP grade groups, growth pattern (expansive vs. infiltrative), tumour area and diameter as well as immunohisto-chemical PSMA heterogeneity, intensity and negative tumour area (PSMA%neg) were correlated with spatially corresponding SUVmax on 68Ga-PSMA-11-PET in a multidisciplinary analysis.
**Results:** All tumours showed medium to strong membranous (2–3 +) and weak to strong cytoplasmic (1–3 +) PSMA expression. Heterogeneously expressed PSMA was found in 38 cases (61 %). Twenty-five cases (40 %) showed at least 5 % and up to 80 % PSMA%neg. PSMA%neg, infiltrative growth pattern, smaller tumour area and diameter and WHO/ISUP grade group 2 significantly correlated with lower SUVmax values. A ROC curve analysis revealed 20 % PSMA%neg as an optimal cutoff with the highest sensitivity and specificity (89 % and 86 %, AUC 0.923) for a negative PSMA-PET scan. A multiple logistic regression model revealed tumoural PSMA%neg ($p < 0.01$, OR = 9.629) and growth pattern ($p = 0.0497$, OR = 306.537) as significant predictors for a negative PSMA-PET scan.
**Conclusions:** We describe PSMA%neg, infiltrative growth pattern, smaller tumour size and WHO/ISUP grade group 2 as parameters associated with a lower 68Ga-PSMA-11 uptake in prostate cancer. These findings can serve as fundament for future biopsy-based biomarker development to enable an individualized, tumour-adapted imaging approach.

## P 20
## Classification of lung cancer metastases in lymph nodes using a multiple instance learning approach*

Mauro Gwerder[1], Amjad Khan[1], Inti Zlobec[2], Christina Neppl[1]

[1]Institute of Pathology, University of Bern, Bern, Switzerland [2]Universität Bern, Bern, Switzerland

**Background:** Identification of possible lung cancer metastases in lymph nodes is needed for pN-staging and further treatment plans. There is a potential for computer-aided metastasis detection on whole slide images (WSIs). However, the required annotations for such cases are cumbersome and tedious for pathologists. We thus propose a weaklysupervised learning approach, by utilizing only global WSI-labels with no regional annotations.
**Methods:** The classification of 293 WSIs from a total of 66 lung cancer patients was performed by an experienced pathologist. The slides were stained with Hematoxylin and Eosin. Training data consists of 205 slides, while 44 slides each were set aside for validation and testing. Tiles of size 256 × 256px were passed through two ImageNet pretrained neural networks (ResNet18 and ResNet34) to select the N tiles per slide with the highest probability for tumor-tissue (N = 1, 10). These relevant tiles were then selected and augmented for model fine-tuning. Augmentation includes random cropping, resizing, color jittering and blurring to avoid overfitting. This two-step process was then repeated until convergence. For each slide, the prediction was decided based on the tiles with the highest probability for having aberrant tissue. The models were evaluated using accuracy and the area under the ROC-curve (AUC) was calculated.
**Results:** A fine-tuned ResNet18 yielded a model with an accuracy of 84.1 % and an AUC of 96.3 % on the test set. Upon increasing the number N of relevant tiles included in training from one to ten accuracy slightly decreased to 81.9 % (AUC of 96.28 %). The same tests with different ResNet34 models returned worse results with accuracies of 75.% (AUC of 82.4 %) for $N = 1$ and 50 % (AUC of 71.7 %) for $N = 10$.
**Conclusions:** Our experiments show that neural networks trained on unrelated, domain-distant data can be fine-tuned to effectively extract relevant features of whole-slide images.
* Student paper

## P 21
## BRAF-mutated histiocytic/dendritic cell sarcoma developing 18 years after a clonally-related follicular lymphoma

Claire Royer* [1], Bettina Bisig[1], Mounir Trimech[1], Edoardo Nissiglia[1], Voruz Sophie[2], Alban Denys[3], Michel Duchosal[4], Anne Cairoli[4], Laurence de Leval[1]

[1]Institut universitaire de pathologie, Centre Universitaire Vaudois, Lausanne, Switzerland [2]Service d'Hématologie, Centre Universitaire Vaudois, Lausanne, Switzerland [3]Service de radiodiagnostic et radiologie interventionnelle, Centre Universitaire Vaudois, Lausanne, Switzerland [4]Department of Hematology, University Hospital Basel, Switzerland

**Background:** Histiocytic/dendritic cell sarcomas (HDS) are uncommon aggressive neoplasms that arise de novo or in association with lymphoid malignancies. Besides recurrent mutations in the RAS/MAPK pathway, secondary HDS show additional genetic alterations typically encountered in the underlying lymphoma, providing evidence of a shared clonal origin. We report an intriguing case of follicular lymphoma (FL) relapsing 18 years after initial presentation under the guise of an HDS.
**Methods:** IG clonality assays, BCL2 break-apart FISH and targeted NGS (customized 54-gene B-cell lymphoma panel) were performed on both HDS and FL.
**Results:** A 1941-born man was diagnosed in 2003 with classical grade 1–2 BCL2+ FL on a mesenteric lymph node excision, with no additional treatment. In 2021, abdominal pain and B symptoms prompted PET-CT investigations and discovery of a hypermetabolic mesenteric mass. A needle biopsy revealed a proliferation of large pleomorphic tumor cells in a reactive background, with atypical mitoses and necrosis. Immunohistochemically, tumor cells were positive for CD45, CD43, CD4, CD1a, S100 and HLA-DR, negative for CD68 (KP1 and PGM1), CD163, langerin, lysozyme and B-cell markers, leading to a diagnosis of HDS. BCL2 and BRAF V600E were strongly expressed. Genetically, the HDS harbored monoclonal IGH and IGK gene rearrangements, but comparative FL analysis was inconclusive. FISH and NGS showed identical alterations typical of FL in both tumors: rearrangement and somatic hypermutation of BCL2, and KMT2D and MEF-2Bmutations. Finally, BRAF V600E mutation was confirmed in the HDS but absent in the FL.
**Conclusions:** The molecular data prove the clonal relationship between the two neoplasms, supporting the hypothesis of a FL transdifferentiating into a HDS, with 18 years delay and after acquisition of a BRAF V600E mutation. Representing a first documentation in this setting, the patient is showing an overall morpho-metabolic response after two months of dual BRAF/MEK inhibitor therapy.

## P 22
## A novel patient-derived model of sarcomatoid urothelial bladder cancer*

Michele Garioni* [1], Ilaria Alborelli[2], Tatjana Vlajnic[3], Heike Pueschel[4], Hans-Helge Seifert[4], Cyrill A. Rentsch[4], Lukas Bubendorf[2], Clementine Le Magnen[1]

[1]University Hospital Basel, Department of pathology and medical genetics and department of urology; [2]University Hospital Basel, Institute of Medical Genetics and Pathology, Basel, Switzerland [3]University Hospital Basel, Institute of Medical Genetics and Pathology, Basel, Switzerland [4]University Hospital Basel, Department of Urology, Basel, Switzerland

**Background:** Sarcomatoid urothelial bladder cancer (SARC) is a rare variant of bladder cancer that is linked to a poor prognosis. Given its rarity, there is limited knowledge on clinical and pathological features and a lack of experimental models to study the disease pathogenesis. Here, we characterized a patient-derived in vitro model of SARC (SARC-Bs1) and tested its response to clinically-relevant drugs.
**Methods:** We collected a SARC sample obtained from a 73 years old male patient undergoing transurethral resection of the bladder and processed it to generate cluster of cells for culture in Matrigel. Phenotypical characterization was performed through Hematoxylin and Eosin (H&E) staining, immunohistochemical, and immunofluorescence analyses. Genotypical characterization was performed through targeted sequencing (Oncomine Comprehensive Assay Plus, Thermofisher). Drugs were tested at eight different concentrations to determine the IC50for each compound. Cell viability was measured using CellTiter-Glo 3D (Promega) after a 5-day long treatment.
**Results:** SARC-Bs1 cells maintained a steady growth for more than 20 passages (~300 days). H&E and immunofluorescence analysis confirmed the phenotypical similarity between SARC-Bs1 and the original tumor, as shown by the marked expression of the mesenchymal marker Vimentin and the lack of expression of epithelial markers. Moreover, targeted sequencing unveiled a high degree of similarities in the mutational profile of the SARC-Bs1 model and its matched tumor. Mutations were detected in hotspot genes such as TP53, RB1, TERT, KRAS. CNV analysis uncovered a deletion in PTEN, whose loss of expression was confirmed by IHC. Finally, SARC-Bs1 cells exhibited different degrees of response to six standard of care and experimental drugs.
**Conclusions:** We successfully established a patient-derived SARC in vitro model, which recapitulates relevant features of the disease and allows testing the efficacy of clinically-relevant drugs. This tool may be useful for treatment decision of patients affected by this rare variant of bladder cancer.
*Student paper

## P 23
## Multiple instance learning based classification of colorectal cancer lymph nodes*

Amjad Khan* [1], Elias Baumann[1], Mauro Gwerder[1], Annika Blank[2], Felix Müller[1], Huu Giao Nguyen[1], Alessandro Lugli[1], Heather Dawson[1], Jean-Philippe Thiran[3], Inti Zlobec[1]

[1]Institute of Pathology, University of Bern, Bern, Switzerland [2]Institute of Pathology, City Hospital Triemli Zürich, Zürich, Switzerland [3]Signal Processing Lab 5 (LTS5), EPFL, Lausanne, Switzerland

**Background:** Evaluating lymph nodes for potential metastasis is a time-intensive task in the diagnostic routine. Advances in deep learning show promising results in tumor detection, but often require extensive annotations for accurate predictions. Our aim was to classify colorectal cancer (CRC) lymph nodes and identify metastases on highresolution whole slide images (WSI) using slide-level labels.
**Methods:** MIL approach was used to stratify the WSI of CRC lymph nodes into metastasis-positive and negative. MIL, is a supervised deep learning method, assumes that given a bag of examples and one global label, at least one of the examples should be predictive of that label. WSI are split into tiles and grouped into bags with the slide-level label. Bags containing any tile with a tumor are considered positive.
The dataset contains 358 lymph node WSI from 69 CRC patients. The data was balanced by selecting all 73 positive slides and randomly adding 73 negative slides and then split into 80 % training and 20 % test sets. 256×256px tiles were extracted at 0.243 µpp (20X) to train ResNet18. To improve model generalization, tiles were randomly cropped (224×224px) and augmented with color jittering (random brightness, contrast, hue, and saturation) and Gaussian blur.
**Results:** Our classifier achieved 0.924 AUC on a test set of 30 WSI with a small training set of 116 WSIs. Tiles containing tumors were correctly classified as positive and non-tumor tiles as negative with some misclassifications occurring as shown in **Fig. 1**.
**Conclusions:** Our results show that a MIL-based classifier can accurately identify positive and negative lymph nodes without requiring additional extensive annotations. In particular, it can filter out negative samples to reduce pathologists' workload for manual evaluation or be used as a preliminary step in deep learning models for further classification or tumor segmentation.
*Student paper

## P 24
## Pericardial effusion in a patient with chronic myeloid leukemia, BCR-ABL1-positive: a diagnostic challenge

Lucine Christe* [1], Luis Veloza[1], Bettina Bisig[1], Sabine Blum[2], Louis Gros[2], Laurence de Leval[1], Ekkehard Hewer[1]

[1]Institut universitaire de pathologie, Centre Universitaire Vaudois, Lausanne, Switzerland [2]Service d'Hématologie, Centre Universitaire Vaudois, Lausanne, Switzerland

**Background:** Body-cavity based lymphomas are a heterogeneous group of rare non-Hodgkin lymphomas arising primarily in serous cavities and resulting in recurrent effusions. They include EBV-positive pyothoraxassociated lymphoma presenting as a solid mass usually in the pleural cavity associated to an effusion, and primary effusion lymphoma (PEL) which grows in a liquid phase without detectable mass. Besides HHV8-associated PEL, which is a distinct DLBCL entity typically presenting in HIV-positive individuals, HHV8-unrelated PEL-like lymphoma may occur in other clinical scenarios.
**Methods:** a paraffin-embedded cell block was built and used for immunohistochemistry, PCR-based IG clonality assays, break-apart FISH studies and targeted NGS were conducted.
**Results:** A 40 years-old patient diagnosed with CML for 6 years and treated with Dasatinib for 23 months presented light dyspnea and dry cough. An echocardiography showed a pericardial effusion and no pleural effusion. Peripheral blood analysis showed a mild anemia and no blasts. BCR-ABL1 transcripts in peripheral blood were absent.
Cytologically, the pericardical effusion was hypercellular and contained large atypical cells with irregular nuclear contours, prominent nucleoli and abundant cytoplasm, accompanied by numerous small lymphocytes in a necrotic background. By immunohistochemistry, the neoplastic cells were CD20+ CD79a+ MUM1+ BCL2+ MYC+ BCL6–/+ and CD10–. HHV8 (LANA-1) was negative. EBER-ISH for EBV was positive in most cells, with co-expression of LMP1 and EBNA2 proteins (EBV latency pattern III). FISH found no rearrangements of BCL2, BCL6and MYC. NGS found BRAF exon 17 and NOTCH2 exon 26 mutations of uncertain signification.
**Conclusion:** this effusion-based EBV-positive large B-cell lymphoma was categorized as HHV8-unrelated PELlike lymphoma. Dasatinib is a second generation tyrosine kinase inhibitor sometimes associated with pericardial effusion. There have been reports of patients treated by Dasatinib for CML, who developed effusion-based HHV8-negative large B-cell lymphomas and showed variable clinical courses. Follow-up in our patient is short.

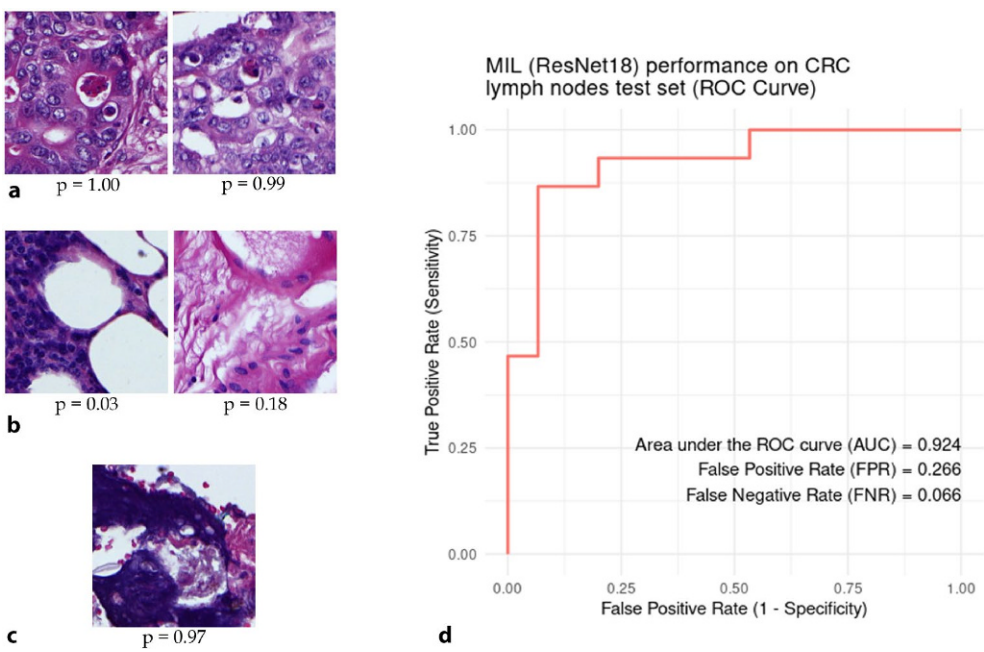


**Fig. 1 | P 23** ◀ Represantative tiles for **a**: true positive, **b**: true negative and **c**: false positive samples from multiple bags)p: probably of a tile containing metastases). Preprocessing artefacts lead to some misclassifications (**c**). **d**: AUC based MIL's performance on the test set

## P 25
## Unusual case of localized crystal-storing histiocytosis complicating primary pulmonary marginal zone lymphoma of mucosa-associated lymphoid tissue (MALT lymphoma) with plasmacytic differentiation

Marie Barbesier* [1], Bettina Bisig[2], Laurence de Leval[2], Sabina Berezowska[3]

[1]Institute of Pathology, Lausanne University Hospital (CHUV) and Lausanne University, Lausanne, Switzerland; [2]Institut universitaire de pathologie, Centre Universitaire Vaudois, Lausanne, Switzerland [3]University of Lausanne, Institute of Pathology, Lausanne, Switzerland

**Background:** Crystal-storing histiocytosis (CSH) is a rare nodular lesion characterized by histiocytes with abundant fibrillary cytoplasmic inclusions representing immunoglobulin light chains, mainly associated with lymphoplasmacytic neoplasms.
**Methods:** A 1.8-cm solitary peripheral pulmonary nodule was resected in a 72-year-old woman with long-standing rheumatoid arthritis, with subsequent histomorphological, immunohistochemical and molecular analyses.
**Results:** Macroscopically, the nodule was tan-white and lobulated, with central necrosis and calcification. Histologically, the nodule consisted predominantly of cytologically bland histiocytes and multinucleated giant cells with needle-shaped cytoplasmic inclusions, accentuated in the Gram stain. Small lymphoid aggregates consisting predominantly of CD20-positive small B cells were present at the border between the histiocytic lesion and the lung, in association with abundant plasma cells showing kappa light-chain restriction, and intimate association with bronchial and alveolar epithelium. A monoclonal IGH gene rearrangement was demonstrated by PCR, in the absence of MALT1 gene abnormalities on FISH analysis. The final diagnosis was a localized crystal-storing histiocytosis complicating primary pulmonary marginal zone lymphoma of mucosa-associated lymphoid tissue (MALT lymphoma) with plasmacytic differentiation. Staging bone marrow biopsy was negative.
CSH can occur in any organ, without gender or age predilection. More than half of the cases present as localized disease, most commonly in the head and neck, lung or pleura. Most cases are associated with plasma cell neoplasms or lymphomas with plasmacytic differentiation. The underlying reason for the tissue phenomenon of CSH is unknown. It is speculated that mutations in the variable region promote conformational alterations of immunoglobulins and lead to crystallization. CSH is not specifically treated. The prognosis depends on the underlying condition.
**Conclusions:** CSH may rarely present as a nodule in the lung, and can partially or completely obscure the presence of an associated or underlying lymphoproliferative disorder.

## P 26
## Digital cytology–a user perspective analysis

Lorenz Buser* [1], Katherine Brandes* [1], Ines Azevedo[2], Pierre Mainil-Varlet[1]

[1]Unilabs, Lausanne, Switzerland [2]Kaizen Institute Portugal, Vila Nova de Gaya, Portugal

**Introduction:** Cervical Cancer remains the fourth most common cancer amongst women worldwide. Cytology has been the gold standard for cervical screening since the introduction of routine screening with the Pap test in the 1950s. Genius Digital Diagnostics System s a CE-IVD marked digital cytology platform to combine a new artificial intelligence (AI) algorithm with advanced volumetric imaging technology to help cytotechnologists and pathologists identify pre-cancerous lesions and cancer cells in women. The system can rapidly analyze all cells on a Thin-Prep® Pap test digital image, narrowing tens of thousands of cells down to an AI-generated gallery of the most diagnostically relevant images.
**Objective:** 1. To validate the Hologic Genius Digital Diagnostic (GDD) system vs. the ThinPrep Imaging System (TIS) and conventional screening with a microscope.
2. To show the GDD system is not inferior to the TIS in identifying abnormal findings.
3. To assess the impact on workflow in a high volume screening laboratory in Switzerland, with the introduction of a digital cytology diagnostic system.
4. To assess user experience and acceptance of digital cytology.
**Method and results:** 5 Cytologists and 2 Pathologists participated in this evaluation.
Cases from our routine workflow collection evaluated in 2020 using the (TIS) system or conventional microscopic evaluation where randomly selected. Abnormal (ASC-US+) and normal slides (fulfilling NILM criteria) were digitized and examined in a blinded second review using solely the GDC system. By using The GDD system we could achieve 91.6 % percent of diagnostic accuracy compared to the TIS. Digital diagnostics could improve Cytologist efficiency by 180 %. Other criteria such as a user-friendly gallery layout, system software, sample traceability, ergonomics, and human fatigue were analysed. The GDD allowed for an improved work environment.
**Conclusion:** Our internal evaluation showed the GDD method can be used for routine diagnostic and improves workflow in the laboratory.

## P 27
## Triple negative breast cancer, a heterogenous group of several entities–differences in h&E based basic criteria like tILs, tumor-budding and mitosis

Lucine Christe* [1], Elisabeth Rönnerman[2], Barbro Linderholm[2], Tilman Rau [1]

[1]Institut für Pathologie der Universität Bern, Bern, Switzerlad [2]Department of Oncology and Pathology, University Gothenburg, Gothenburg, Sweden

**Background:** Triple negative breast cancer (TNBC) is an oncological term and is widely used in literature. Despite major breakthroughs in cancer treatment TNBC still has a bad prognosis with limited targeted treatments. The novel WHO classification of breast tumors 2019 created new separated entities like the apocrine adenocarcinoma, paving the way for a more precise classification of TNBC. However, little is known regarding how much the new entities differ in H&E basic biomarkers like TILs, tumorbudding, mitosis rate or other parameters of the BRE scoring system.
**Methods:** We revised histologically a cohort of 391 patients diagnosed with TNBC collected in the University of Gothenburg for the construction of an ngTMA. Beside immunohistochemistries and essentialcriteria for correct differential diagnosis, we assessed the BRE score with glandular architecture, mitosis, nuclear pleomorphism, tumor infiltrating lymphocytes (TILs) and tumor budding.
**Results:** A number of 55 cases appeared to be positive for either ER, PR or HER2 according to current guidelines and were excluded. Thereafter, the cohort was subdivided in 4 groups: NST ($n = 254$), apocrine adenocarcinoma ($n = 56$), lobular carcinoma ($n = 9$) and rare special type like metaplastic or salivary gland like tumors ($n = 17$). In ANOVA analysis the subgroups differed for mitosis rate, tumorbudding and TILs. Only nuclear pleomorphism and glandular architecture was not significant. In pairwise analysis, the NST group presented with significantly highest mitotic activity and TIL formation.
**Conclusion:** In case of TNBC in daily routine assessment, several deviations in H&E parameters like low TILs and less mitotic activity could be a strong hint for a possible special subtype.